UNIVERZITA KARLOVA V PRAZE
Přírodovědecká fakulta

DIPLOMOVÁ PRÁCE

Eva Pluhařová

Molekulové simulace nukleace ledu

Katedra fyzikální a makromolekulární chemie
Ústav organické chemie a biochemie, AV ČR, v.v.i.

Vedoucí diplomové práce: doc. Mgr. Pavel Jungwirth, DSc.
Studijní program: Chemie, Fyzikální chemie

2010

CHARLES UNIVERSITY IN PRAGUE
Faculty of Science

DIPLOMA THESIS

Eva Pluhařová

Molecular simulations of ice nucleation

Department of Physical and Macromolecular Chemistry
Institute of Organic Chemistry and Biochemistry, ASCR, v.v.i.

Thesis advisor: doc. Mgr. Pavel Jungwirth, DSc.
Specialization: Chemistry, Physical Chemistry

2010

I would like to express my deep thanks to my advisor doc. Pavel Jungwirth for teaching me and guiding me. I would also like to thank all my former and current colleagues for the friendly environment in which I could work and deal with problems. I appreciate access to the METACentrum supercomputing facilities provided under the research project MSM6383917201 and Czech Science Foundation grant P208/10/1724

Finally, I would like to thank my parents who supported me and my studies all the time and also my boyfriend Jan for his tolerance and love.

Prohlašuji, že jsem svou diplomovou práci napsala samostatně a výhradně s použitím citovaných pramenů. Souhlasím se zapůjčováním práce a jejím zveřejňováním.

V Praze dne 30. 4. 2010

Eva Pluhařová

Název práce: Molekulové simulace nukleace ledu
Autor: Eva Pluhařová
Katedra: Katedra fyzikální a makromolekulární chemie PřF UK
Vedoucí diplomové práce: doc. Mgr. Pavel Jungwirth, DSc., ÚOCHB AV ČR, v.v.i.
e-mail vedoucího: pavel.jungwirth@uochb.cas.cz

Abstrakt: Pomocí simulací molekulové dynamiky jsme systematicky studovali homogenní nukleaci ledu v čisté vodě a dále vliv přítomnosti povrchově aktivních látek na tento děj. Jako modely surfaktantů byly použity kyselina pentanová a pentanol. Čistá voda začíná mrznout převážně v podpovrchové vrstě, která se přizpůsobí zvětšení objemu během tvorby ledu lépe než molekuly v objemu kapaliny. Alkohol ovlivňuje homogenní nukleaci více než kyselina. Voda pokrytá neuspořádanou vrstvou pentanolu vykazuje zanedbatelnou preferenci pro podpovrchovou nukleaci a delší nukleační čas ve srovnání s čistou vodou, zatímco přítomnost kyseliny pentanové nesnižuje výrazně podpovrchovou preferenci pro začátek mrznutí ani nemění nukleační čas. Rozdíly mezi vlivem různých funkčních skupin jsme se pokusili vysvětlit na základě jejich schopnosti orientovat molekuly vody a měnit jejich pohyblivost. Skutečnost, že různé surfaktanty mají na homogenní nukleaci ledu různý vliv, je významná z hlediska tvorby mraků ve vyšší vrstvách atmosféry, do níž se během spalování biomasy uvloňuje řada organických látek.

Klíčová slova: molekulová dynamika, empirické potenciály, surfaktanty, homogenní nukleace ledu.

Title: Molecular simulations of ice nucleation

Author: Eva Pluhařová
Department: Department of Physical and Macromolecular Chemistry Faculty of Science UK
Advisor: doc. Mgr. Pavel Jungwirth, DSc., IOCB AS CR, v.v.i.
Advisor's e-mail address: pavel.jungwirth@uochb.cas.cz

Abstract: By means of molecular dynamics simulations we have systematically investigated homogeneous ice nucleation in neat and surface contaminated water. As models of the adsorbates we have assumed pentanol and pentanoic acid. In neat water nucleation preferentially starts in the subsurface region, which accommodates better than the bulk the volume increase associated with freezing. Homogeneous ice nucleation is affected more by alcohol than by acid. Water slabs covered by a disordered layer of pentanol exhibit negligible preference for subsurface nucleation and longer nucleation times in comparison with neat water, while nucleation times are almost unaffected by the presence of pentanoic acid and the subsurface preference is only slightly decreased. We tried to rationalize the differences between the effects of different compounds by their ability to orient water molecules and to change their mobility. The fact that adsorbates differ in the influence on homogeneous ice nucleation has important implications for the microphysics of formation of high altitude clouds upon conditions when a wide range of high molecular weight compounds is emitted to atmosphere during biomass burning.

Keywords: molecular dynamics, empirical potentials, surfactants, homogeneous ice nucleation.

Contents

Chapter 1

Introduction

Water is a unique substance which occurs in all three phases under natural conditions. An elaborate equation of state has been developed for water due to its importance in industry. Its phase transitions have been investigated in great detail, including rather complicated solid phase regions with several forms of ice crystal structures [1]. As other systems, water does not necessarily have to be in the equilibrium state, i.e. in the global minimum of the Gibbs free energy surface, but it can also be in a metastable state. Such examples are supercooled liquid or supersaturated vapour, both playing an important role in the physics of atmosphere. Each phase scatters and absorbs light differently, so the total Earth's radiation budget is influenced by the phase composition of clouds, which, due to the existence of metastable phases, cannot be determined simply from the equilibrium phase digram based on temperature and pressure. The transformation into a stable phase has to proceed via nucleation process which is connected with a barrier, since creation of a new interface requires energy. A nucleus of a new phase can be formed via random fluctuations or the transformation may happen with the help of some other particle. The first process refers to homogeneous, the latter to heterogeneous nucleation. For better understanding and consequent modelling of atmospheric processes, it is necessary to know the mechanisms of formation of stable phases and there are still many open questions in this field [2].

Water in nature mostly freezes heterogeneously; in the atmosphere on dust particles and on the ground in contact with inorganic minerals or even on living organism, particularly bacteria which are efficient ice nuclei, now employed also for commercial purposes. Although most of the ice in the world is formed by heterogeneous processes, homogeneous ice nucleation has also received a lot of attention, since it controls formation of tropospheric cirrus, polar stratospheric clouds, and thunder-

clouds [3, 4, 5, 6]. It is still not clear, whether homogeneous freezing of small droplets is a volume or surface controlled process [7]. Therefore, in our group we decided to study this process with molecular resolution by means of classical molecular dynamics with empirical potentials. In case of small droplets, it is highly probable that freezing starts from the area close to the surface, so it can be affected by surface pollution, for example by amphiphilic compounds which are present in the atmosphere due to forest fires and anthropogenic emissions [8].

This thesis is based on a pioneering study of homogeneous ice nucleation from 2002 [9], and more directly on the first simulations of such process in slabs of water, i.e. at the air water/interface [10]. Homogeneous ice nucleation is a random process, proper description of which requires a set of nucleation events. The goals of this thesis are: (i) to study homogeneous ice nucleation in neat water employing molecular dynamics simulations and bring statistics into this issue, (ii) to investigate the effect of surface pollution, represented by an aliphatic acid and alcohol, on this process (iii) to compare investigated systems in terms of nucleation times and location of ice nucleus, and (iv) to explain eventual differences by analysis of obtained trajectories.

This work is organized as follows. The second chapter describes ice nucleation in the atmosphere and how it can be studied experimentally and theoretically. The computational method used in this work, i.e. classical molecular dynamics with empirical potential, is outlined in chapter 3. In the fourth chapter, I specify model systems and simulation protocol. Chapter 5 provides results and plausible explanations of observed phenomena and chapter 6 summarizes results and discusses possibilities for future studies.

Chapter 2

Ice nucleation in neat and polluted water

This chapter, which provides a short literary survey, starts with definition of terms connected with ice nucleation, both heterogeneous and homogeneous. Then, I describe where these processes occur in nature and why they are important especially for physics and chemistry of the atmosphere. For atmospheric modelling, it is necessary to understand individual process, therefore, experiments on model system under well defined conditions are needed. The third section introduces laboratory experiments and in the last section, I mention computational studies of homogeneous ice nucleation and also the effect of amphiphilic molecules on freezing.

2.1 Thermodynamic approach, classical nucleation theories

This section is based on a previously published review [7]. All liquids can be cooled bellow their melting point, T_m. The temperature of T_m is defined by thermodynamics as the temperature where the liquid and crystalline phases can coexist in equilibrium with each other at given pressure. Above T_m the liquid is the stable phase, below T_m the crystal is the stable phase (left part of Fig. 2.1). A liquid below T_m is in a metastable state, which means in a local minimum in the Gibbs energy landscape, while the absolute minimum corresponds to the stable crystalline phase.

The temperature at which freezing actually occurs in real samples is determined by kinetics and involves a nucleation process, which was mentioned in the previous chapter. Heterogeneous nucleation is depicted in the middle of Fig. 2.1, while homoge-

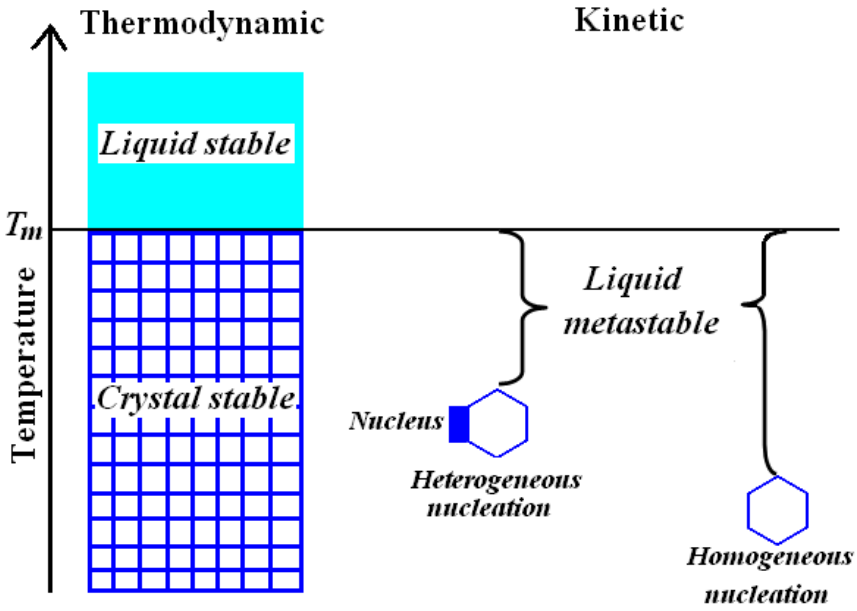

Figure 2.1. Schematic picture comparing different nucleation mechanisms for the freezing of a liquid. T_{m} is the melting point of the crystalline phase. Adopted from [7].

neous nucleation is presented in the right part. Under otherwise identical conditions, heterogeneous nucleation always occurs at a higher temperature than homogeneous nucleation. This is generally true, because the addition of foreign nuclei to a liquid can only enhance the overall nucleation probability. Therefore, homogeneous nucleation serves as the lower temperature limit to which a liquid can be supercooled. The homogeneous ice nucleation temperature T_{hn} is a genuine property of the metastable liquid and for pure water it is about 235 K. Heterogeneous nucleation occurs anywhere between T_{hn} and T_{m} and it strongly depends on the suitability of a particular nucleus.

Ice nucleation is a stochastic process. The first theoretical description of crystallization of supercooled water droplets into ice was presented by Volmer [11]. He considered a sample that consists of m water molecules each of which has a probability p to become the center of a critical nucleus. For large m and $p << 1$, nucleation rate ω of the whole sample can be defined:

$$\omega = \frac{mp}{t} \quad , \tag{2.1}$$

where p/t is the nucleation rate for a single molecules in the sample. The probability

that a sample remains unfrozen after time t_n is:

$$P(t_n) = \exp(-\omega t_n) \quad . \tag{2.2}$$

The freezing rate ω depends on parameters such as temperature and sample size and it can be written as a product of homogeneous nucleation rate coefficient and sample volume $\omega = J(T) \cdot V$.

Recently, Tabazadeh and coworkers suggested that liquid-to-solid nucleation occurs preferentially at the surface and not in the interior [8, 12, 13]. A necessary condition for surface nucleation reads as:

$$\sigma_{\mathrm{vs}} - \sigma_{\mathrm{vl}} < \sigma_{\mathrm{ls}} \quad , \tag{2.3}$$

where σ_{vs}, σ_{vl} and σ_{ls} refer to vapor-solid, vapor-liquid and liquid-solid surface tension, respectively. If the condition is fulfilled, the probability for a water molecule at the droplet surface to become the center of a critical germ, p_{S}, is larger that of a molecule in the interior of the droplet, p_{V}. Taking into account surface-dependent nucleation, the equation 2.1 can be rewritten as:

$$\omega = \omega_{\mathrm{S}} + \omega_{\mathrm{V}} = \frac{m_{\mathrm{S}} p_{\mathrm{S}}}{t} + \frac{m_{\mathrm{V}} p_{\mathrm{V}}}{t} = J_{\mathrm{S}} \cdot S + J_{\mathrm{V}} \cdot V \quad , \tag{2.4}$$

where S and V are total collective surface are and volume, respectively, of all droplets. It is not *a priori* clear whether volume- or surface-dependent mechanism dominates, it also strongly depends on the droplet size.

Water in nature does not occur as a pure species, but it dissolves many compounds. Solutes affect the equilibrium and non-equilibrium properties of water. The depression of the equilibrium melting temperature is one example. Similarly, the kinetic non-equilibrium process of ice nucleation is also affected by the presence of solutes. Based on experimental data, Rasmussen suggested that the homogeneous freezing temperature depression ΔT_{hn} and equilibrium melting point depression ΔT_{m} are linearly correlated [14]. To account for solute effect, several theories have been developed, the most successful being the water-activity-based ice-nucleation theory. Theoretical description of heterogeneous nucleation is more difficult. It also uses water activity as one input for parametrizing this process in aqueous droplets for atmospheric purposes. The effect of solutes and ice nuclei is also important in cryobiological applications, because ice nucleation in biological systems is predominantly heterogeneous.

2.2 Ice nucleation in the atmosphere

For almost 200 years, persistent (liquid) fogs have been observed at temperatures well below the frost point, and there has been a vigorous interest in understanding why, and how far can water droplets supercool in the atmosphere [8]. Radiative properties of clouds and their subsequent effect on climate depend strongly on the size of the cloud particles and their phase [6]. The latter is also crucial for rates of chemical reactions, which occur in cloud droplets or on cloud surfaces. It is important for us to be able to predict, whether droplets are liquid or solid. Note, there is not "one" solid phase, but several forms of ice.

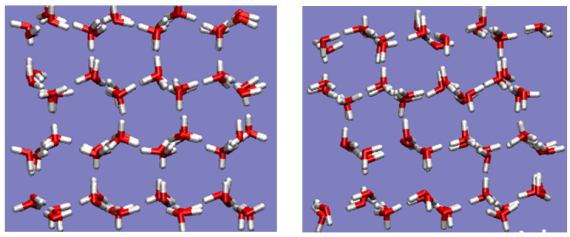

Figure 2.2. Comparison of the structures of hexagonal and cubic ice.

The usual form obtained by freezing of water at atmospheric pressure is the hexagonal ice I_h. Other phases are produced by the application of high pressures, which results in denser packings of molecules [1]. Based on the phase diagram, it was assumed that in the Earth's atmosphere hexagonal ice is formed [6]. However, it has been reported and demonstrated experimentally, that a metastable crystalline phase of ice, cubic ice I_c may form in the atmosphere at temperatures bellow 190 K [15]. Structures of above mentioned ice phases can be seen in Figure 2.2. This should be taken into account in atmospheric modelling, since cubic ice has higher vapor pressure and different heterogeneous chemistry due to the different binding sites [15].

The presence of heterogeneous ice nuclei (IN) in supercooled water droplets is necessary for glaciation of clouds at temperatures above the homogeneous ice nucleation threshold (ca. -38 °C). Interest in materials that are effective as ice nuclei started in the early 1940s with the discovery that natural supercooled clouds can be modified and possibly stimulated to produce precipitation by seeding with silver iodide and other species [16]. A recently regained interest in atmospheric particles on which ice crystals can form is due to their control of cloud microstructure and consequent effects on the cloud radiative properties. There is a great variety of naturally

occurring or man-made atmospheric aerosols that can constitute relatively effective atmospheric IN (AIN). Among the natural AIN, there are inorganic nuclei originating from sources such as soil or volcano dust as well as macromolecules from different biological systems. Plants constitute a nonnegligible direct source of ice nucleating airborne bacteria. The bacteria are transported into the surface boundary layer and could be mixed throughout the depth of the troposphere. The IN of bacterial origin are the most active nuclei that have been identified. In their nucleating potency they exceed by far the more extensively studied silver iodide. Bacteria of the type *Pseudomonas syringae* are now commercially employed as IN for artificial snow. However, on the basis of the sparse results obtained so far, there is no evidence of a substantial contribution of materials of biogenic origin to the AIN population, and the importance of the role of biogenic AIN has not been convincingly demonstrated yet. Some specific anthropogenic activities, such as extensive burning of vegetation, space shuttle launching, or certain industries have been documented as the AIN sources [2, 16].

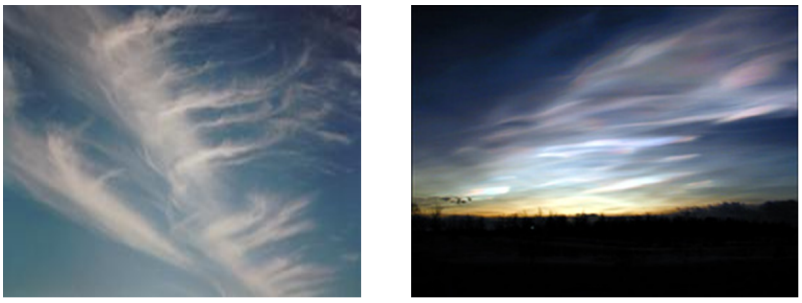

Figure 2.3. Tropospheric cirrus and polar stratospheric clouds.

Ice particle number densities in clouds below -30 °C are often observed to exceed the ice nuclei number densities [3]. This indicates that, in clouds, some supercooled water droplets freeze homogeneously. In addition, it has been shown that freezing in the polar stratosphere occurs via a homogeneous nucleation process, which is also important for formation of tropospheric cirrus (Fig. 2.3) and thunderclouds [3, 4, 5, 6]. Therefore, it is important to elucidate the actual physical process by means of which clouds glaciate in the atmosphere, particularly at cold temperatures and in situations where IN become less abundant and less effective [8]. It is not clear, whether freezing start from the bulk or close to the surface of water droplets [7]. The fact that atmospheric droplets may begin to crystallize at their surfaces makes this process sensitive to the surface coverage. Anthropogenic emissions, which are

often rich in low surface tension components, can condense on pre-existing particles and may change the rate of surface crystallization in the atmosphere. Some of the organic molecular markers identified in atmospheric aerosols are long chain fatty acids, n-alkenals, long chain alkenones, n-alkanols, n-alkanes, and polycyclic aromatic hydrocarbons [17].

2.3 Laboratory experiments

Measurements on supercooled water are difficult to perform because of the likelyhood of ice nucleation to occur in samples of normal size and purity [18]. One strategy to prepare liquid samples devoid of any ice nuclei is dividing a bulk sample into numerous small compartments. As a result, only a minor fraction of the small samples contain ice nuclei, while most of others are free of them. Therefore, only a small number of samples freeze heterogeneously, but the majority of the samples freezer homogeneously. Such samples may be small water droplets in oil, in the so called emulsion technique. Differential scanning calorimetry of emulsified samples is particularly successful for measuring the homogeneous freezing temperature of aqueous solutions [7]. Other experimental investigations of freezing of smaller water droplets in the micrometer and even nanometer size range involve electrodynamic free-fall tubes [19], levitation traps [20, 21], and jet expansions [22].

In the first approach, about 5 droplets per second are ejected from a generator at the top of a temperature controlled freezing tube. They fall in a stream down the center of the tube and their images are recorded using video-telemicroscopy. The fraction of droplets frozen is measured as a function of height (and, hence, as a function of temperature) by illuminating slices of the stream with linearly polarized laser light and monitoring the depolarization of the backscattered light; ice particles depolarize the scattered light while liquid droplets do not. The homogeneous freezing temperature was determined to be -37 °C.

The measurements of levitating droplets are carried out using single weakly charged microdroplets of water which are levitated under a controlled atmosphere in an electrodynamic trap. The liquid/solid phase transition is detected by analyzing the scattered light from a laser. The homogeneous nucleation rate coefficient, which strongly depends on temperature, varies from (10^6 [21] - 10^7 [20]) $cm^{-3}s^{-1}$ at -36 °C to (10^7 [21] - $5 \cdot 10^8$ [20]) $cm^{-3}s^{-1}$ at -37 °C for droplets having tens of μm in diameter. However, the homogeneous ice nucleation rate coefficient obtained by jet expansion technique for droplets containing 4000-6000 molecules was determined to be up to

10^{24} $cm^{-3}s^{-1}$ [22], which is about 20 orders of magnitude bigger than in the case of previously mentioned studies. For droplets with a diameter between 1-5 mm situated in an acoustic levitator, high-speed monitoring of the freezing process was reported recently [23]. In this approach, combined visual (VIS) and infrared (IR) imaging directly delivers three-dimensional and surface temperature information about the proceeding freezing front with up to two thousand frames per second.

Homogeneous nucleation rate coefficients differ for different experimental techniques, furthermore, it is still not clear whether they should be obtained from volume- or surface dependent nucleation theory. From measurements employing the method of electrodynamical levitation, Duft et al. concluded that homogeneous ice freezing is a volume-proportional process with surface nucleation being potentially important for small droplets with radii below 20 μm [24]. Volume nucleation is more probable for bigger droplets simply because many more molecules are present in the bulk than in the surface layer (see eq. 2.4). On the other hand, Tabazadeh et al. found that in some emulsion experiments the presence of surfactants at the oil/water interface prevents surface nucleation [12]. In these cases volume nucleation is the favoured nucleation process. But for droplets in air, they suggested that surface nucleation dominates. There is still debate about this topic, since neither of the mechanisms is fully supported due to the scatter in experimental results obtained by different techniques.

Heterogeneous ice nucleation has been also studied extensively [2]. The complex structure as well as the chemical diversity of natural IN complicate theoretical descriptions of the ice nucleation process. It has been suggested that ice-nucleation substrates bear surfaces that match the crystal structure of ice and thus serve as templates that induce nucleation by epitaxy. Another mechanism which invokes the presence of local electric fields that are capable of aligning water molecules into ice-like embrii has been proposed [25]. One strategy of investigating the relationship between structure of the IN and its activity is to employ model substances that mimic the properties of natural IN. One such a type of IN are self-assembling amphiphilic molecules at the surface of water droplets [26]. These molecules forming a Langmuir layer may be designed such that their hydrophilic head groups create a surface or template similar to a layer of the to-be-nucleated crystal. Furthermore, by modifying the hydrophobic tail, it is possible to vary, albeit within limits, the packing arrangement of the head groups and, consequently, directly influence the kinetics of crystal nucleation, as well as the type of the crystal nucleated under monolayer [25].

The activity of these monolayers as ice nucleators is evaluated by measuring the threshold freezing temperatures of supercooled water drops covered by the mono-

layers [25]. For example induced freezing of drops of supercooled water covered by ordered monolayers of long chain (i.e., with more than 10 CH_2 groups) aliphatic alcohols and carboxylic acids was extensively studied [25, 26, 27, 28, 29, 30, 31, 32]. The ice-nucleation temperatures were found to depend on the length of the hydrocarbon chain and the even-odd parity of carbon atoms, as well as on the chemical nature of the headgroup. A systematic increase in nucleation temperature was found for long chain alcohols (but not carboxylic acids) starting from about 15 carbon atoms [27].

2.4 Computer simulations

The first step in computational modelling is to a choose reasonable model system and an appropriate level of theory. Classical molecular dynamics with empirical potentials is now the only possibility for studying homogeneous ice nucleation, since it is a stochastic process and it is necessary to collect a sufficient number of long trajectories. The choice of an empirical potential is not straightforward; many of them exist for water, but only a few of them were parametrized for simulation of liquid water/ice coexistence. Even adjustment of melting temperature close to experiment was done only recently. Next, it would be also beneficial, if the water model is compatible with available models for other species, such as ions or small organic molecules. This topic will be discussed in more details in section 4.1, here I just briefly mention previous computational studies concerned with homogeneous ice nucleation and related topics.

The first successful homogeneous ice nucleation trajectory was obtained in 2002 by Matsumoto et al. [9]. It was performed for bulk water, i.e., without the air-water interface, employing the TIP4P water model [33]. The melting temperature of TIP4P is about 40 K lower than experimental value, thus a better model for ice simulations was needed. Nada and van der Eerden developed a six-site water model (NE6) particularly for simulations of supercooled water and ice around melting point [34]. This model was used to study ice growth from supercooled water in contact with crystalline ice [35, 36] and even in presence of an anti-freeze protein [37]. In our group, we decided to use this model for homogeneous ice nucleation in a slab of water, i.e., with the air/water interface, since it is interesting from the atmospheric perspective. Slabs of neat water of varying thickness were simulated and, based on six nucleation trajectories, it was concluded that homogeneous freezing starts preferentially just below the surface layer [10]. One nucleation trajectory was obtained also for a salt solution and nucleation time was in this particular case ten time longer than in neat

water [23], which is in accordance with the well known anti-freeze effect of salt.

The effect of adsorbates on ice growth has also been studied previously. These studies have been mainly concerned with long-chain alcohol monolayers covering water [38, 39]. Due to the computational demands, special methods of propagation (reversible reference system propagation algorithm) [38] or simplification of description of alcohols [39] have been used. These studies successfully explain how the orientation of head groups in the monolayer affects the adsorbate/ice/water interface, but they do no target time evolution of such systems.

Based on the literary survey, only a handful of homogeneous ice nucleation trajectories was collected up to now. That is why the main goal of this work was to draw conclusions about ice nucleation in neat water from a larger set of trajectories and then to study the effect of surface pollution.

Chapter 3

Classical molecular dynamics

This chapter provides a brief overview of the theoretical method which was employed in this thesis, i.e., the classical molecular dynamics. It starts from statistical thermodynamics, basic terms of which are mentioned in section 3.1. Then, I describe a typical way, how interactions and movements of molecules are treated. Next, I outline some "technical tricks" that have to be employed in the simulations and finally I discuss what can be extracted from computer experiment. Definitions and notation were adopted from the literature, [40, 41, 42, 43, 44].

3.1 Statistical thermodynamics

Fenomenological thermodynamics is based on several axioms resulting from observations of nature. It provides us with many useful relations between measurable quantities of macroscopic systems, but it does not have any tool for determination of concrete values of these characteristic quantities. It considers the system as a black box without a microscopic structure. On the other hand, the goal of statistical thermodynamics is to determine thermodynamic quantities based on interactions between particles constituting the system [40]. The state of a classical system can be completely described by specifying the positions and momenta of all particles. System of N particles is thus characterized by $6N$ coordinates. The $6N$-dimensional space defined by these coordinates is called the phase space, every point of which is a microstate. Over time, a dynamical system maps out a trajectory in the phase space. The trajectory is a curve formed by the phase points the system passes through. Sometimes, by trajectory we mean a curve formed by points in the $3N$ dimensional configurational space. A thermodynamic system is fully characterized by a few independent thermodynamic quantities, e.g., number of particles N, temperature T, and

volume V. An ensemble is a set of all microstates, which are compatible with given thermodynamic state of the system. Depending on, how the system is defined, the following ensembles can be distinguished: NVE, NVT, NpT or μVT.

Letting A be a macroscopic quantity which evolves in time, the average quantity $\langle A \rangle_\tau$, called the time average is defined as:

$$\langle A \rangle_\tau = \frac{1}{\tau} \int_0^\tau A \left(\boldsymbol{r}^N(t), \boldsymbol{p}^N(t) \right) \, \mathrm{d}t \quad . \tag{3.1}$$

An ensemble-averaged quantity is defined as:

$$\langle A \rangle_{ens} = \int \int A \left(\boldsymbol{r}^N, \boldsymbol{p}^N \right) P \left(\boldsymbol{r}^N, \boldsymbol{p}^N \right) \mathrm{d}\boldsymbol{r} \mathrm{d}\boldsymbol{q} \quad , \tag{3.2}$$

where $P \left(\boldsymbol{r}^N, \boldsymbol{p}^N \right)$ is the probability of being at a particular phase space point. This probability depends on the energy associated with the phase point according to Boltzmann's law, which for the NVT ensemble reads:

$$P \left(\boldsymbol{r}^N, \boldsymbol{p}^N \right) = Q^{-1} \exp \left(-E \left(\boldsymbol{r}^N, \boldsymbol{p}^N \right) / k_\mathrm{B} T \right) \quad . \tag{3.3}$$

Here, k_B is the Boltzmann's constant, Q is the system partition function, and E is the total energy. According to a common assumption that the potential energy U does not depend on momenta, E can be written as follows:

$$E \left(\boldsymbol{r}^N, \boldsymbol{p}^N \right) = K \left(\boldsymbol{p}^N \right) + U \left(\boldsymbol{r}^N \right) \quad . \tag{3.4}$$

where K is the total kinetic energy. If τ in eq. 3.1 is sufficiently long, i.e. that system gets arbitrarily close to any microstate, then $\langle A \rangle_{ens} = \langle A \rangle_\tau$. This is valid for the so called ergodic systems. The ergodic hypothesis allows us to evaluate thermodynamic quantities of the system from the sufficiently long MD trajectory.

3.2 How to describe movement of molecules

Before we start any computer simulation, we have to know how particles which constitute the system interact with each other. According to the Born-Oppenheimer approximation, we can treat "fast" electrons and "slow" nuclei separately; nuclei then move on the so called potential energy surface (PES) and electrons adjust infinitely fast. How to construct PES? Of course, it would be ideal to take solution of

the Schrödinger equation, but this is usually not feasible due to the computation demand. Therefore empirical potentials are typically used. The form of the interaction potential is usually given as:

$$U = \underbrace{E^{\text{bond}} + E^{\text{angle}} + E^{\text{dihe}}}_{\text{intramolecular}} + \underbrace{E^{\text{vdw}} + E^{\text{Coulomb}}}_{\text{intermolecular}} \quad . \tag{3.5}$$

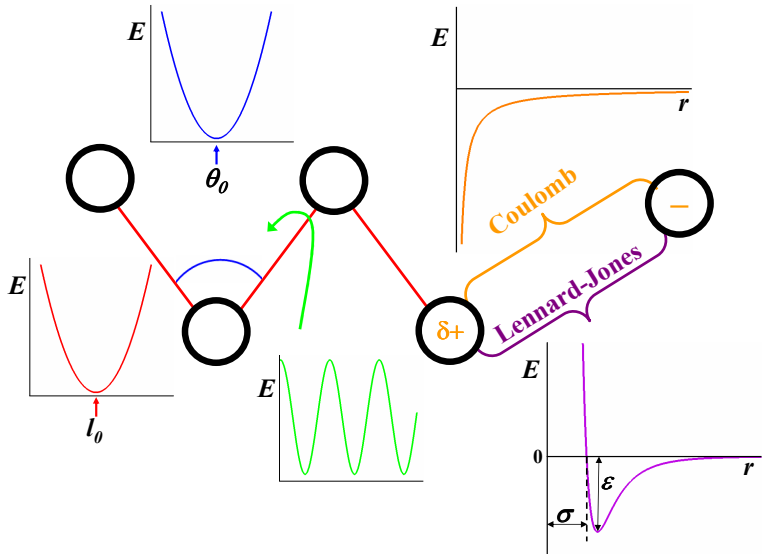

Figure 3.1. Intramolecular and intermolecular energy contributions described by molecular mechanics.

This expresses the molecular potential energy as a sum of intramolecular energy terms which describe the distortions of bond lengths, bond angles, and torsion angles away from equilibrium values, and intermolecular terms for pairs of atoms describing van der Waals and electrostatic interactions. The set of parameters consisting of equilibrium bond lengths, bond angles, force constants, van der Waals parameters, partial charge values, and other parameters is called a force field. The bond and angle intramolecular terms within harmonic approximation read:

$$E_i^{\text{stretch}} = \frac{k_i}{2}(l_i - l_{i,0})^2 \tag{3.6}$$

$$E_i^{\text{bend}} = \frac{\beta_i}{2}(\theta_i - \theta_{i,0})^2. \tag{3.7}$$

where $l_{i,0}$, $\theta_{i,0}$ are the optimal bond length and angle. The force constants, k_i, β_i, determine the strength (rigidity) of the bond or angle. The harmonic approximation is sufficient under usual conditions, because deviation from equilibrium values are not large. Since the torsion itself is periodic, so must be be the torsional potential energy:

$$E_i^{\text{dihe}} = \frac{1}{2}\sum_n V_n[1 + (-1)^{n+1}\cos(n\omega_i + \omega_{i,n})], \tag{3.8}$$

where V_n is equal to the maximum energy by which the particular term can contribute, n is the periodicity of the term, the factor of $(-1)^{n+1}$ is included so that the function in brackets is zero for all n when $\omega_i = \pi$, if the phase angles $\omega_{i,n}$ are zero. This is due to the empirical observation that most torsional energies are minimized for antiperiplanar (trans) geometries.

The intermolecular N-body term is usually approximated by the sum of two-body terms:

$$E_{ij}^{\text{Coulomb}} = \frac{1}{4\pi\epsilon_0}\frac{q_i q_j}{r_{ij}}, \tag{3.9}$$

$$E_{ij}^{\text{vdw}} = 4\epsilon_{ij}\left[\left(\frac{\sigma_{ij}}{r_{ij}}\right)^{12} - \left(\frac{\sigma_{ij}}{r_{ij}}\right)^{6}\right]. \tag{3.10}$$

The electrostatic interaction is expressed by the Coulomb law. Charges q_i in eq. 3.9 are integers in case of ions or non-integers in case of atoms in molecules. The van der Waals (repulsion-dispersion) interaction is often used in the form of the Lennard-Jones 12-6 potential (eq. 3.10), defined by atom-type-dependent constants σ_{ij} and ϵ_{ij}, the meaning of which is depicted in Fig. 3.1 For short distances it generates a strongly repulsive force caused by overlaying of electronic clouds, while for larger distances it causes attraction which comes from induced dipole-induced dipole interactions. More sophisticated force fields contain also other terms such as polarizabilities, which account for changing partial charges due to interaction with surrounding, special terms for hydrogen bonds, etc.

Up to now, I have described widely used functional forms for description of interaction between molecules, but did not mention, how to obtain system-specific parameters. This is done via optimization procedures. We have a set of molecules and a set of unknown parameters and target properties which we want to reproduce. From those, a penalty function is constructed and parameters are obtained by minimizing this function. Employing this approach, unphysical results could be

obtain, therefore, a so-called physically-controlled fit is performed in order to obtain reasonable numbers. It is beneficial to use information not only from the condensed phase, but also from spectroscopic experiments and *ab initio* calculations for isolated molecules and small clusters.

Once we define the parameters in the above equations, our system is completely determined. At this point we can in principle evaluate system partition function and from it determine thermodynamic quantities. This is, however, almost impossible due to the dimensionality of the problem. A better option is to let the system evolve in time according to Newton equations and then by the use of the ergodic hypothesis evaluate time averages of the quantities. The Newton equations read:

$$m_i \ddot{\boldsymbol{r}}_i = \boldsymbol{f}_i, \tag{3.11}$$

where forces $\boldsymbol{f}_i$ acting on the atoms are derived from the interaction potential $U(\boldsymbol{r}^N)$,

$$\boldsymbol{f}_i = -\frac{\partial U(\boldsymbol{r}^N)}{\partial \boldsymbol{r}_i} \quad . \tag{3.12}$$

Here $\boldsymbol{r}^N = (r_1, r_2, \ldots r_N)$ represents the complete set of $3N$ atomic coordinates. Equations of motion are not solved analytically, but numerically. Several methods of numerical intergration exist, e.g. Runge-Kutta, Gear, but the most widely used one is the Verlet algorithm because of its simplicity and time-reversibility. It is more stable with longer time step comparing to the other integrators. Verlet propagation with time step δt reads:

$$\boldsymbol{r}_i(t+\delta t) = 2\boldsymbol{r}_i(t) - \boldsymbol{r}_i(t-\delta t) + (\delta t)^2 \frac{\boldsymbol{f}_i(t)}{m_i}. \tag{3.13}$$

3.3 Realization of a pseudo-experiment

Realization of a computational experiment depends on the character of the problem. If we model a dynamical (nonequilibrium) problem, the simulation protocol is as follows:

set of inital conditions → set of MD trajectories → analysis.

Since from one trajectory we can not predict anything meaningful in case of a dynamical process, it is necessary to simulate many trajectories and "average" over them. The distribution of positions and velocities in the of set of initial conditions

should correspond to the distribution in real experiment. Trajectory long enough to cover the process is generated for different initial conditions.

In case of an equilibrium process, where we use MD trajectory for sampling the equilibrium ensemble, the simulation protocol reads:

initial condition → equilibration → MD trajectory → analysis.

The initial geometry can be guessed, taken from a database or from minimization of the former. Velocities are usually taken from the Maxwell-Boltzmann distribution at a given temperature. A system obtained in this way is not in equilibrium; a short equilibration before the production run is therefore necessary. MD trajectory then samples an equilibrium ensemble and according to ergodic hypothesis, we can obtain thermodynamic properties from time-averages.

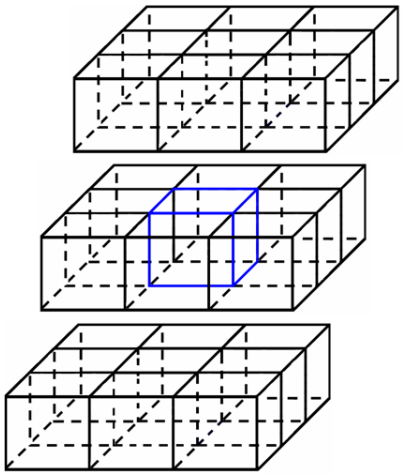

Figure 3.2. Periodic boundary conditions.

With common force fields, systems containing thousands of atoms can be studied. This is enough for isolated systems (molecules and clusters), but not enough for studying condensed phases. To remove surface effects,the so called periodic boundary conditions (PBC) are applied. This means that a finite system under consideration is placed in a box, by replicating of which the whole space can be filled. It is illustrated in Figure 3.2, where blue cube refers to the original system. All particles in replicas move identically with the particles in the original system. Particles can leave the cell and at the same time its image enters the simulations cell from the opposite site. Forces acting on every particle in the original cell are calculated only from nearest non-identical neighbours which are situated either in the central cell or in surrounding cells. This is called the minimum image convention.

More than 90% of computation time is spent on evaluation of forces, therefore, as little as possible of contributions is evaluated. Short range interactions, i.e. decaying faster than r^{-3}, such as those from the Lennard-Jones potential can be cut off (set to zero) at certain distance r_c. This causes a jump in forces, which is sometimes corrected using a switch-function or simply by shifting the whole function. The cut-off approach can not be used for long-range interactions, such as ion-ion, ion-dipol, and dipol-dipol interaction, which have to be summed over all periodic images. Special methods have to be used, such as the Ewald summation or reaction field method, the latter being applicable only for systems without ions.

To obtain a trajectory as long as possible with given amount of computational resources, we try to use a reasonably long time step δt in eq. 3.13. However, at the same time it should be short enough to properly describe the fastest motion in the system and to ensure stability of the propagation scheme. If we "freeze" the fastest motion in the system, typically vibrations of bonds with hydrogen atoms, we can increase the time-step and also avoid problems with quantum nature of these vibrations. There are two popular algorithms for constraining bonds: SHAKE [45] and LINCS [46]. The latter consists of the following steps: at first, new positions of atoms are obtained from Newton equations without applying any restrictions, next the bond length is set to desired value without changing the direction of the bond and finally a correction is applied for the lengthening of bonds due to rotation. This procedure allows to use typically a time step of ~ 2 fs.

Newton equations of motion conserve total energy, so without including any other terms, the microcanonical ensemble is generated. However, in usual applications we are interested in NVT or NpT ensembles. In case of PBC we obtain a constant volume automatically due to the fixed cell size, but temperature has to held constant using some trick. The easiest, but the most crude way is to rescale velocities at every step by (T/T_{kin}), where T is the desired temperature and T_{kin} is kinetic temperature. Berendsen improved this approach by adding friction term into Newton equations of motion. The advantage of these methods is their simplicity and fast convergence, but they do not exactly generate a canonical ensemble. The exact canonical ensemble can be obtained using Andersen's thermostat or by adding artificial degrees of freedom. The former from time to time actualizes velocity of one particle with the new velocity taken from the Maxwell-Boltzmann distribution. This can be interpreted as interaction with a thermostat. The latter introduces a thermal reservoir into the Lagrangian of the system via additional degree of freedom with corresponding thermal inertia.

3.4 What does MD tell us?

MD program packages provide us with the set of positions and velocities for every atom at each time step, but unfortunately, we don't know much more about the investigated problem after performing the simulation. We need to extract a representative information that it easy to understand or visualise, such as how one property depends on one or two variables.

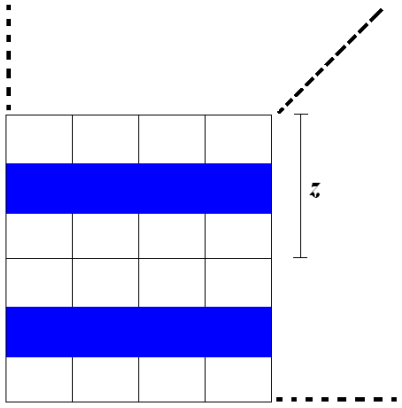

Figure 3.3. Noninteracting slabs formed by periodic repetition of cell prolonged in z direction.

In this work, the slab geometry was employed, this means that the system is placed in a rectangular cell prolonged sufficiently in one direction (z in Figure 3.3) and replicated in all three directions as is depicted by dashed lines. By this, noninteracting infinite slabs of water in our case are obtained. Distribution of species along the slab does not necessarily have to be uniform. Some species may have surface preference, others can be depleted from the interfacial layer. It is beneficial to depict partial densities of individual atom types or groups of them. Illustration of such a density profile is provided in Figure 3.4, where density of oxygen atoms is plotted against z-axis. In case of liquid water (black line), we can see a constant value with smooth transition at the air/water interface, while for ice (red line), there are regions of low and high density due to the crystal structure. Note, that for monitoring of the freezing process, we can investigated evolution of density profile in time.

To quantify distribution of particle B around particle A, radial distribution function $g_{AB}(r)$ is commonly used, which is defined in the following way:

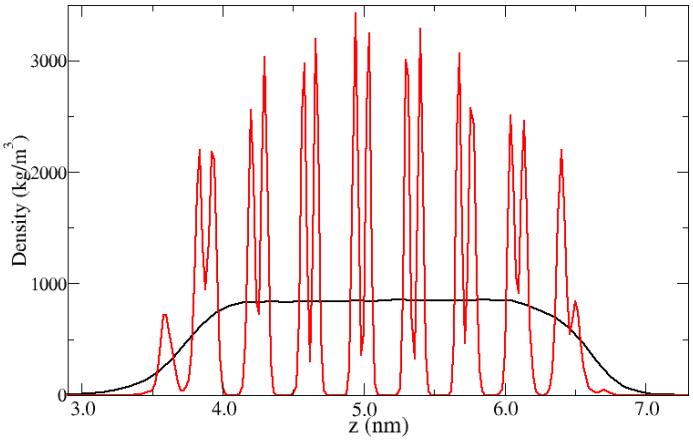

Figure 3.4. Density of water oxygen plotted against z axis for liquid (black line) and ice (red line).

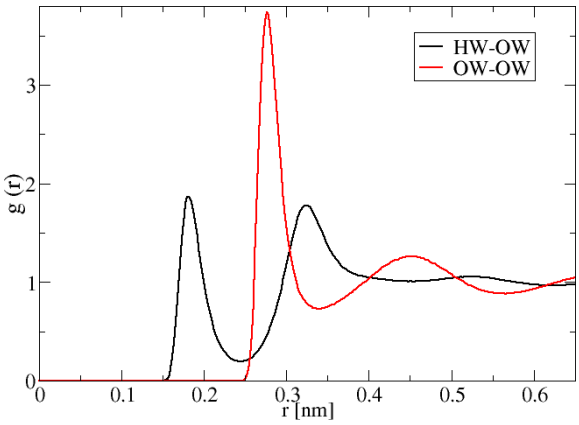

Figure 3.5. Radial distribution function of hydrogen-oxygen (black) and oxygen-oxygen (red) of NE6 water model [34].

$$g_{AB}(r) = \frac{\langle \rho_B(r) \rangle}{\langle \rho_B \rangle} = \frac{1}{N_A \langle \rho_B \rangle} \sum_{i \in A}^{N_A} \sum_{j \in B}^{N_B} \frac{\delta(r_{ij} - r)}{4\pi r^2}, \tag{3.14}$$

where $\langle \rho_B(r) \rangle$ is the particle density of type B at a distance r around particles A, and $\langle \rho_B \rangle$ the average particle density of type B. Radial distribution of water hydrogens (black) around water oxygens (red) in NE6 water is depicted in Figure 3.5. The first maximum of hydrogen-oxygen distribution occurs at 0.18 nm and the first minimum at 0.25 nm, while for oxygen-oxygen the first maximum is present at 0.28 nm and the first minimum at 0.34 nm. Locations of minima are important for a geometrical

definition of a hydrogen bond, which is has the OH distance shorter than 0.25 nm or the OO distance shorter than 0.35 nm and the HOO angle smaller than 30°.

The so-far mentioned analyses did not carry time information. This is included in time correlation functions, which describe how the value of quantity $A(\xi)$ at time ξ correlates with the value of quantity $B(\xi + t)$ at time $\xi + t$:

$$C_{AB}(t) = \langle A(\xi)B(\xi + t)\rangle_{\xi}\,, \tag{3.15}$$

where $\langle\rangle_{\xi}$ means averaging over ξ. If A equals to B, C_{AB} is called the autocorrelation function. Time correlation functions give us an idea about dynamical connections between studied quantities, i.e., after how long time, a change in one quantity does not affect the other any more.

Chapter 4

Simulation

This chapter provides specific description of model systems, force field parameters of individual molecules, and details about propagation of the Newton equations of motion. Special attention is paid to selection of water model, since there is a plethora of water force fields each of which is good for some purposes, but fails in description of other phenomena. All MD simulations were performed using the Gromacs program package; the majority of calculations was performed using version 3.3 [47] and the last few trajectories in version 4 [48]. *Ab initio* calculations, which were done in order to check qualitative behaviour of empirical potentials, were performed employing Gaussian 03 program package [49].

4.1 Force fields

We should keep in mind that description of the system by the employed methodology is only approximative and our results cannot be better than the force field. We have to choose a model that was fitted to reproduce properties which we want to study. This work is concerned with freezing of water (also in contact with other species), so our model of choice should reproduce melting temperature and phase digram of water at ambient conditions. The strength of interaction of adsorbate molecules with each other and also with water should be at least semi-quantitatively correct.

4.1.1 Water

In usual MD simulations water is treated as a rigid molecule with a negative partial charge located at or close to the oxygen and with positive charges on hy-

drogens. A Lennard-Jonnes interaction site is situated on the oxygen atom and for some models also on hydrogens. A water model can be polarizable or non-polarizable; for simplicity I will focus on the latter. The development started from an intuitive picture of water, having three interaction sites, such as the SPC [50], SPC/E [51], and TIP3P [52] models. When the negative charge is moved from the oxygen slightly towards hydrogens, but the LJ parameter remains on oxygen, the TIP4P model [33] is obtained. In spite of its simplicity, TIP4P describes the phase diagram of water relatively well. It was further improved and TIP4P-like family of water models now contains TIP4P/Ice [53], TIP4P/2005 [54] developed by Vega and coworkers, and TIP4P-Ew [55]. The second way of development is to add additional interaction sites. In case of the TIP5P model [56], the negative charge is situated on the lone electron pairs. The six site interaction potential NE6 has the negative charge distributed between lone-pairs and an extra point located in the H-O-H bisector. The positive charge is placed on the hydrogens.

As was mentioned above, TIP4P is able to reproduce the shape of the phase diagram of water including several ice phases, but it is shifted to lower temperatures by 40 K. TIP4P/2005 provides on average the best description of most of water properties, but its melting temperature T_{m} differs from experiment by about 20 K. The fact that also other popular models underestimate the melting point is not a big problem if the pure substance is investigated. As a first approximation, the simulation temperature is shifted by the difference between model and experimental T_{m}. But this probably would not work, if other species are present. That is why we need a model with correct melting temperature. The second reason is that molecules are moving slowly at low temperatures. It would take long time for molecules to rearrange and form ice, so the resulting nucleation times will not be accessible by our simulations. TIP5P and TIP4P/Ice [53] reproduce the experimental T_{m}. The former has a reasonable diffusion coefficient, but does not reproduce the phase diagram, the opposite is true for the latter model. The other candidate is NE6. In the original paper, it was reported that its melting temperature is 275 K [34], but then it was corrected by the authors to the range of 280-285 K [57]. The melting temperature of this model was recalculated again by two methods: a combination of a Gibbs-Duhem integration and free energy calculations and the determination of the melting temperature by direct coexistence of water and ice. The final results is 289 K [58], which is 16 K higher than the experimental value, but this is an acceptable deviation, if we compare it with other models. Moreover, Carignano pointed out that NE6 crystallizes faster than other models [36], which is an advantage for this study.

NE6 water model with abbreviations for interaction sites is depicted in Figure

Table 4.1. Intermolecular force field parameter of NE6 water model [34].

Name	Atomic weight	Partial charge [e]	σ [nm]	ϵ [kJ·mol^{-1}]
OW	15.999	0.000	0.3115	0.715
HW	1.008	0.477	0.067	0.115
EP	0.000	-0.866	0.000	0.000
LP	0.000	-0.044	0.000	0.000

4.1, force field parameters are summarized in Table 4.1. Oxygen and hydrogen atoms carry mass and LJ interaction parameters. Hydrogens also have charges, while oxygen does not. Oxygen charge is distributed on virtual sites with zero mass.

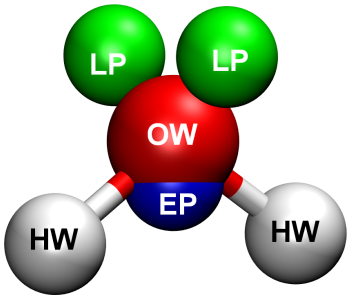

Figure 4.1. NE6 water model [34] with following abbreviations of interaction sites: oxygen (OW), hydrogen (HW), lone electron pair (LP), extra point (EP).

4.1.2 Pentanoic acid

Force field parameters for pentanoic acid were obtained as a combination of *ab initio* based results and values provided in standard force field Amber parm99 [59]. At first, I optimized the structure at MP2/aug-cc-pVDZ level and then carried out population analysis according to the Merz-Singh-Kollman scheme [60], which fits electrostatic potential by partial charges at selected points. These charges serve as input for one subroutine in Amber program package [59], which derives partial charges using restrained electrostatic potential approach (RESP). Finally, other non-bonding and bonding parameters are taken from parm99 [59] database. Force filed parameters for pentanoic acid employed in this work are provided in Table B.1.

Parameters for water and pentanoic acid were obtained by different procedures and to match different target properties. So, there is a question about using them

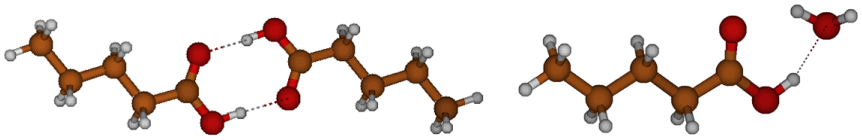

Figure 4.2. Pentanoic acid dimer a) and pentanoic acid water dimer b).

Table 4.2. Interaction energies of pentanoic acid dimer and pentanoic acid water pair in MP2 geometries in kJ·mol^{-1}, notation taken from Figure 4.2.

	a)	b)
MP2/aug-cc-pVDZ	71.5	39.5
Empirical potential	68.4	41.7

together. NE6 is a non-polarizable water model, optimized to reproduce certain bulk properties. But for example, for NE6 water dimer, I obtained interaction energy of 26.5 kJ·mol^{-1} which is larger than MP2 result of 18.7 kJ·mol^{-1} calculated in this work and MP2 reference value 21.0 kJ·mol^{-1} [61]. Due to hitting bulk properties with fixed charge distribution, common non-polarizable models overestimate interaction energies in small water clusters. For purpose of this work, reasonable description of interaction energies between water and pollutants is needed. So I checked interaction energies of pentanoic acid dimer with two strong hydrogen bonds (Figure 4.2 a)) and pentanoic acid-water heterodimer with one strong and one weak hydrogen bond (Figure 4.2 b)) obtained at MP2/aug-cc-pVDZ level with empirical results. Corresponding values of systems in MP2 geometry are summarized Table 4.2. Empirical and *ab initio* energies are in reasonable agreement, so no further refinement was done.

4.1.3 Pentanol

Parameters for pentanol were obtained and checked in the same way as for pentanoic acid. Two pentanol molecules form a dimer with one hydrogen bond, which is additionally stabilized by van der Waals interactions of aliphatic chains as can be seen in Figure 4.3 a). There are two pentanol-water heterodimers with one hydrogen bond. In the first one with stronger interaction, water acts as hydrogen donor, while

the second one, where pentanol acts as hydrogen donor, has lower interaction energy.

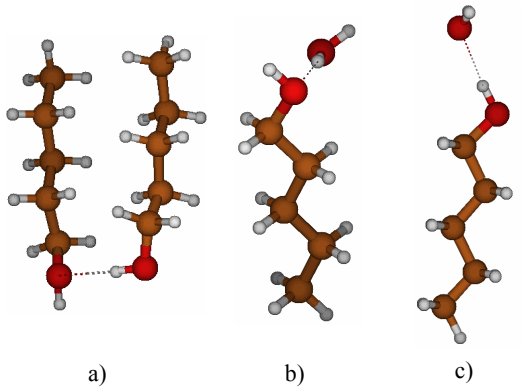

Figure 4.3. Pentanol dimer a) and pentanol water dimers b), c).

Interaction energies of these clusters in MP2 geometries are provided in Table 4.3. As can be seen in the second row, empirical potential based on the RESP charge fitting and Amber parm99 [59] gives opposite order in the interaction energies of the heterodimers. This problem has already been mentioned [39]. In order to obtain correct order of the interaction energies of investigated clusters, I slightly modified the force-field parameters. To decrease the ability of pentanol being hydrogen donor, the positive charge on pentanol OH hydrogen was reduced and the absolute value of negative charge of oxygen was increased. The rest of the positive charge was distributed on alkyl hydrogens. This charge modification resulted in decrease of interaction energy of pentanol dimer, therefore, the LJ parameter ϵ was increased to bring it back, close to the original value. Interaction parameters for pentanol are given in Table B.3, values before modification are given in Table B.2 for comparison.

Table 4.3. Interaction energies of pentanol dimer and pentanol water pairs in MP2 geometries in kJ·mol^{-1}, notation taken from Figure 4.3.

	a)	b)	c)
MP2/aug-cc-pVDZ	32.2	23.5	18.3
Emp. potential based on [59]	30.8	26.3	28.9
Modified emp. potential	30.4	26.8	21.8

4.2 System preparation

Homogeneous ice nucleation is a rare event, therefore long trajectories are needed to study this process. To make the simulation feasible, relatively small systems are investigated. The exact dimensions of the simulation cell, can not be chosen randomly, since the crystal, which is the result of the simulation has to fit in. The preparation of the smallest system under study is depicted in Figure 4.4. It starts with a small piece of proton disordered hexagonal ice I_h with dimensions of 13.5×15.5×29.5 Å^3 containing 192 water molecules, which is placed into a rectangular cell prolonged in the z-direction to 100 Å(Figure 4.4 b)). This system is replicated in all three direction resulting in infinite non-interacting ice slabs. Obtained system is heated up to 300 K and melted; the resulting simulation cell can be seen in Figure 4.4 c). Surface pollution is modelled by adding six adsorbate molecules on each surface, which form an incomplete disordered layer (Figure 4.4 d)).

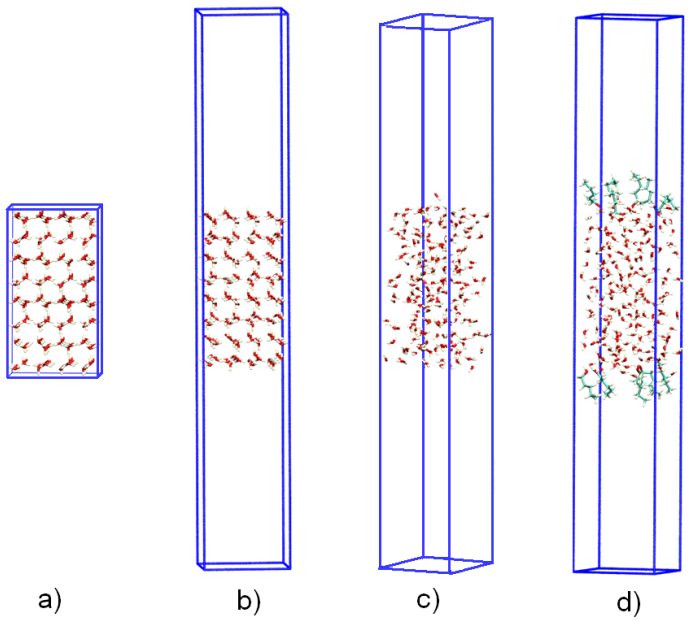

Figure 4.4. Preparation of the smallest system under study a) crystal of hexagonal ice I_h, b) crystal of hexagonal ice in rectangular cell with dimensions of 13.5 × 15.5 × 100 Å^3, c) water slab, and d) slab of polluted water.

The resulting water slab is thick enough to provide a well developed bulk region, as concluded in [62, 63] from studying the air/liquid interface. Mainly based on hydrogen bond analysis (calculating hydrogen-bonded neighbours), it was suggested, that the shortest distance from the vapour/liquid interface to reach bulk behaviour

is $\sim$ 10 Å. During the simulation, the slab thickness slightly fluctuates, the resulting thickness of the bulk being 10-12 Å. As surface, we consider the first layer, which has 3-4 Å, the rest of the interfacial layer we call subsurface, having roughly comparable volume to the bulk. Note, that this separation is based not only on geometrical criteria, but also on hydrogen bond network analysis [62, 63].

Thicker slabs having the same lateral dimension have been also studied. They were prepared in the same way, except for starting from ice crystal having two or three times larger z dimension placed in a 180 or 270 Åthick rectangular cell. The lateral dimension of the cell is relatively small and may cause some artefacts, therefore I also tried to simulate a system duplicated in x and y directions.

4.3 Simulation protocol

Simulations have been performed in the NVT ensemble. The number of particles as well as volume were defined in the previous section. Temperature has been determined in a previous study [10] - by tests at temperatures between 240 and 260 K, 250 K was chosen. Initial coordinates were obtained from the last frame of a "melting" trajectory and velocities were taken randomly from Maxwell-Boltzmann distribution at $\mathrm{T} = 10\,\mathrm{K}$. During 0.4 ps, the system is gradually heated to 250 K, which is followed by short equilibration period of 4.6 ps at this temperature, that is maintained by Berendsen thermostat [64] with short coupling constant of 0.1 ps. The production trajectory is collected at the same temperature using the Nose-Hoover thermostat [65] a with 0.5 ps coupling constant. Note, that Gromacs user works with the period of the oscillation of kinetic energy between the system and the reservoir, not with the "mass" of the reservoir. Bonds containing hydrogen were constrained employing the LINCS algorithm [46]. Due to the small lateral dimensions of the cell, non-bonded interactions were cut-off at 6.5 Å. Long range electrostatic interactions were accounted for using the smooth particle mesh Ewald method, using a pseudo-2D correction for the slab geometry [66]. Newton equations of motion were propagated with a time step of 1 fs for hundreds of ns depending on the nucleation time.

Chapter 5

Results and Discussion

This chapter reports about observed ice nucleation in MD simulations. It starts with illustrative snapshots from nucleation trajectories, then it quantifies the influence of surface pollution on the onset of freezing and finally, it tries to explain observed phenomena based on several types of analyses.

5.1 Monitoring nucleation

In this work, I have collected more than 15 nucleation trajectories for the smallest slab of each system and due to the computational demand only up to 3 trajectories for thicker slabs. Four snapshots from a successful nucleation trajectory for the smallest slab of each system under study are shown in Figure 5.1; presenting neat water (top), water covered by pentanoic acid (middle), and water covered by pentanol (bottom). Only the unit cells, containing 192 water molecules and, in the latter two cases also the 12 adsorbate molecules, are depicted. The newly formed ice nucleus is highlighted by a transparent oval. In the selected trajectory for neat water, nucleus was formed in the subsurface region after ∼160 ns. In water covered by pentanoic acid it also formed in the subsurface after ∼250 ns, while in water covered by pentanol it took ∼380 ns to form a nucleus close to the center of the slab. Figure 5.2 provides snapshots from one simulation of the thickest slab of each system. In the presented trajectory of neat water, ice nucleus was formed in the subsurface region after ∼52 ns. Since ice here does not grow in contact with crystal template, its structure contains defects. One such defect can be formation of five-member and seven-member ring, as can be seen in black ovals in the last snapshot. In selected trajectories of surface contaminated water, ice nucleus was formed in the bulk region, it took ∼67 ns in case of water covered by pentanoic and ∼13 ns in case of water covered by pentanol.

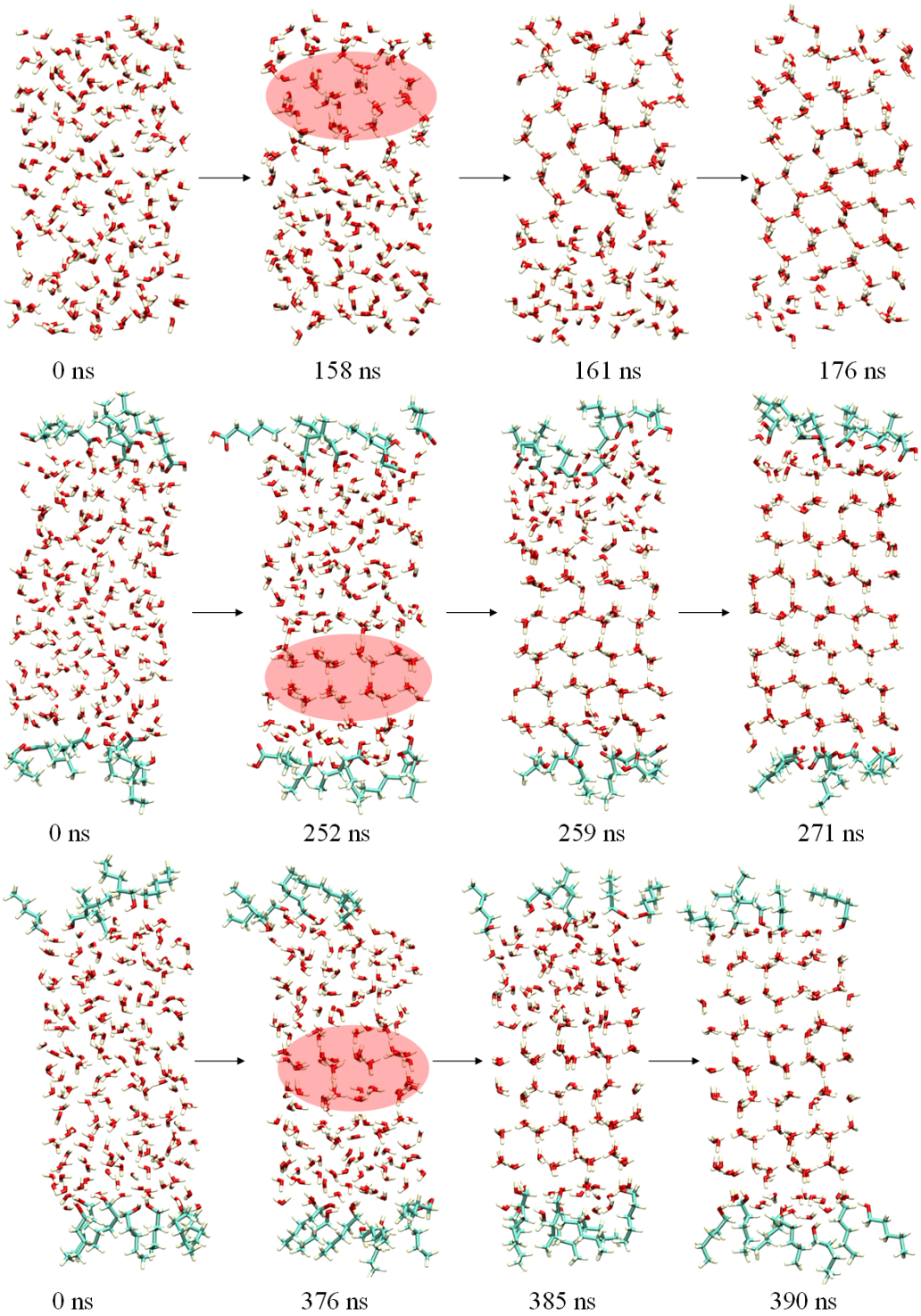

Figure 5.1. Four snapshots from a selected nucleation trajectory for the smallest slab of each system under study: neat water (top), water covered by pentanoic acid (middle), and water covered by pentanol (bottom).

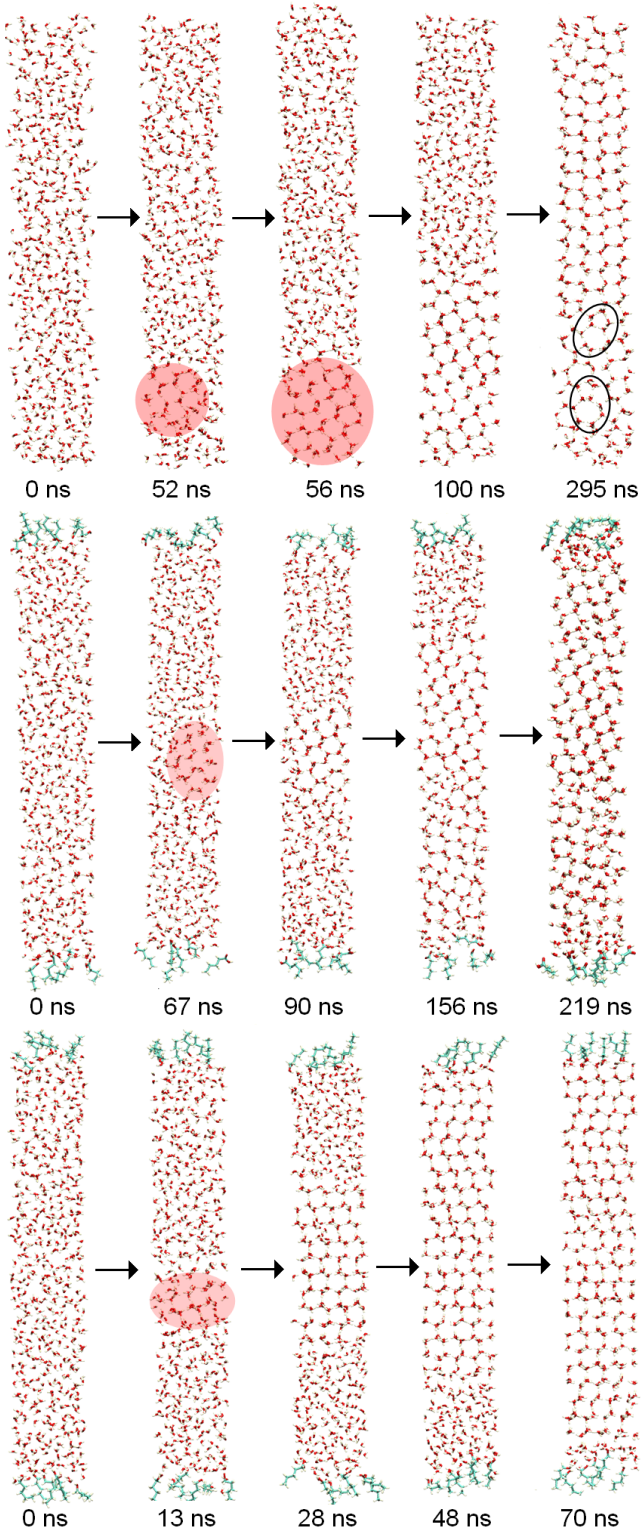

Figure 5.2. Five snapshots from a selected nucleation trajectory for the thickest slab of each system under study: neat water (top), water covered by pentanoic acid (middle), and water covered by pentanol (bottom).

For the thickest slab containing neat water, I have obtained three trajectories; freezing started in the subsurface region twice. For the thickest slab of polluted water, the same number of nucleation events have been collected for both adsorbates, but freezing started from the subsurface once for the alcohol as well as for the acid. In case of medium size slabs, I have obtained the same result for neat water and water covered by pentanoic acid as in the thickest case, but in case of medium size water slab covered by pentanol, I have observed only two nucleation events, both occurring in the subsurface. Results for the systems of the smallest size are discussed in more details in the next section.

The onset of crystallization can be monitored in several ways: 1. observing formation of six-membered rings, 2. searching for "long lasting" hydrogen bonds between four-coordinated water molecules, 3. by the decrease of potential energy of the system and 4. based on the evolution of density profiles in time. The first approach was illustrated in Figures 5.1 and 5.2. The second and the third one were suggested by Matsumoto et al. [9], and the last approach was presented in [67]. In the first panel of Figure 5.3, there are snapshots from one nucleation trajectory for neat water, molecules depicted as green spheres are those which form four "long-lasting" hydrogen bonds (with longer life-time than 2 ns). Blue arrows point to the simulation time, at which the snapshot was taken. The evolution of potential energy of the system is plotted in the middle panel. It is roughly constant until about 210 ns, then it is decreasing for about 15 ns, while freezing proceeds, and finally it is roughly constant again. The bottom panel shows the evolution of density profile of water oxygens (in $\mathrm{kg{\cdot}m^{-3}}$) during simulation, blue color correspond to the low density, red correspond to the high density. If only liquid water is present at a given time, the density profile is the same as the black curve in Figure 3.4. The density is constant across the slab at a value which corresponds to the yellow color in Figure 5.3. If also crystal is present, there are regions of low density (blue) and high density (red), as can was illustrated by the red curve in Figure 3.4. According to the evolution of density profile, freezing also started at about 210 ns and finished at about 225 ns.

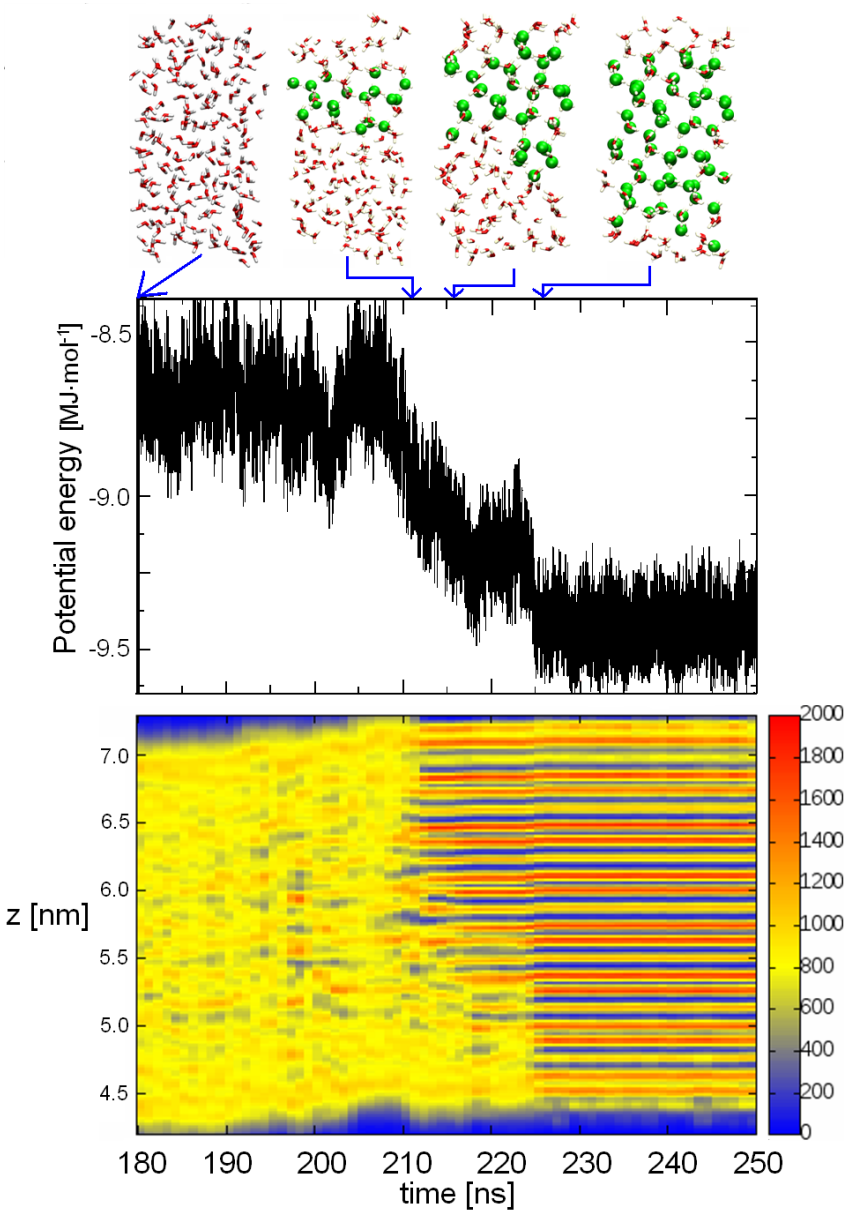

Figure 5.3. Monitoring crystallization by several approaches: long-lasting hydrogen bonds (top), evolution of potential energy during simulation (middle), and evolution of density profile in time (bottom). Colour coding corresponds to the density of water oxygens.

5.2 Analysis of trajectories according to the nucleation theory

To investigate homogeneous ice nucleation according to the nucleation theory, one needs more than a handful of nucleation events. In order to obtain more trajectories with given computational resources, simulations of the smallest system, which has comparable volume of bulk and subsurface regions, were performed. Figure 5.4 shows in a compact form results for neat water, it plots the fraction of slabs without nucleus against time. Green empty circles depict the onset of freezing in the subsurface, while filled green circles correspond to bulk nucleation. The location was determined according to the distance of newly formed six-membered rings from the interface or, if this was not unequivocal, based on the location of the first tetracoordinated water molecule with long-lasting hydrogen bonds. The analysis is based on 17 nucleation trajectories. As can be seen in Figures 5.4 and 5.5, freezing starts preferentially in the subsurface region (subsurface to bulk ratio of 12:5).

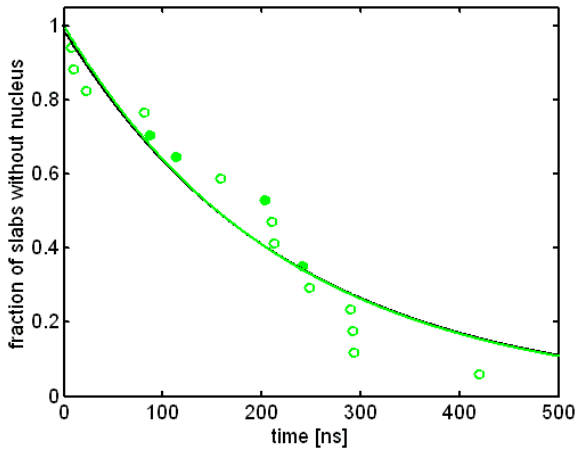

Figure 5.4. Fraction of neat water slabs without an ice nucleus plotted against time. Empty green circles correspond to a nucleus formed in the subsurface, while filled circles represent a nucleus formed in the bulk region. Black and green curves represent two-parameter and one-parameter fits.

This conclusion is in accord with the previous study [10] and also agrees with results for thicker slabs, which are, however, only qualitative due to a small number of trajectories. The subsurface preference can be explained by the interplay between two effects. On one hand, volume increases during freezing, therefore, its onset should be preferred in the region with lower density, i.e. in the surface layer. On the other

hand, for formation of a stable ice nucleus, "long-lasting" hydrogen bonds are needed, but these cannot be formed directly at the surface, since water molecules here are undercoordinated and more mobile. This remains true even after almost the whole slab is frozen, surface molecules form a so called "quasi-liquid" layer.

Location of the newly formed ice nucleus is one important observable, the next one is nucleation time. Based on equation 2.2 it can be obtained from an exponential fit of pseudo-experimental data, even though they are not perfectly exponential. Extracted nucleation time τ equals to $1/\omega$. I have performed a two-parameter least-square fit of data $k{\cdot}\exp(-t/\tau)$ represented by the black curve and also a one-parameter fit $\exp(-t/\tau)$ represented by the green curve, τ refers to the nucleation time. One parameter fit was performed, since the curves should start at the point [0,1].

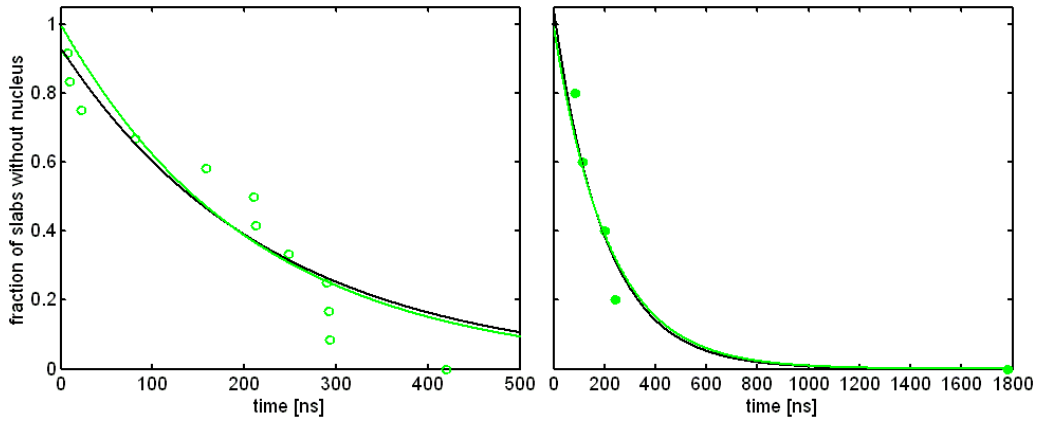

Figure 5.5. Fraction of neat water slabs without an ice nucleus plotted against time separately for subsurface and bulk nucleation. The left part corresponds to the subsurface nucleation, the right part to the bulk one. Black and green curves represent two-parameter and one-parameter fits.

Although, the data set is not large, I tried to separate the subsurface and bulk nucleation events into two plots as if they belonged to different systems. The left part of Figure 5.5 displays fraction of slabs without the nucleus, where subsurface nucleation occurred. The right part displays the same quantity for slabs, where freezing started from the bulk. The points are fitted in the same way as in the previous plot. Nucleation times obtained from previously mentioned fits are summarized in Table 5.1. The values resulting from one-parameter and two-parameter fit are close to each other, although not exactly the same, the most pronounced difference occurs in separate fit for subsurface nucleation. One-parameter fit predicts shorter nucleation times for separate cases than for the total one, this is not qualitatively correct, but the

difference is not dramatic. To conclude, based on our data and taking into account the imperfection of the fits, it seems, that subsurface and bulk nucleation occur on similar time scales. For further discussion, I will use 220-230 ns as nucleation time in slabs of neat water.

Table 5.1. Nucleation times for all neat water slabs and for subsurface and bulk nucleation separately in ns.

	all	subsurface	bulk
1-parameter fit	224	211	213
2-parameter fit	228	230	200

The effect of adsorbed acid on the ice nucleation kinetics is presented in Figures 5.6 and 5.7, which were constructed in the same way as in case of neat water. Empty symbols (red triangles) again correspond to the subsurface nucleation, while filled to the bulk one. As can be seen from these figures, 16 nucleation trajectories were collected. This system again exhibits subsurface preference for formation of the ice nucleus, but it is slightly decreased in comparison with neat water (subsurface to bulk ratio of 10:6). Black and red curves represent two- and one-parameter fits, respectively, the corresponding nucleation times being provided in Table 5.2.

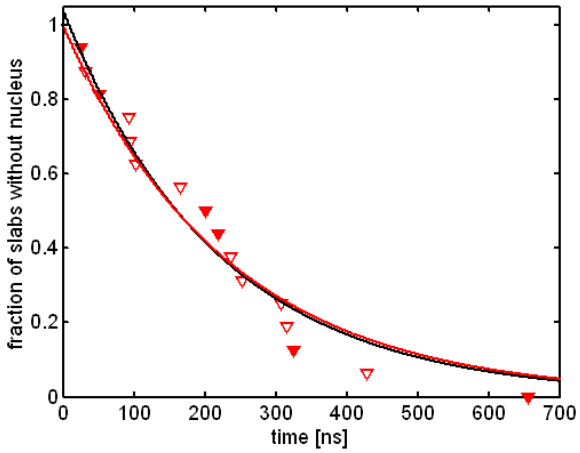

Figure 5.6. Fraction of slabs of water covered by pentanoic acid without an ice nucleus plotted against time. Empty red triangles correspond to a nucleus created in the subsurface, while filled triangles represent a nucleus formed in the bulk region. Black and red curves represent two-parameter and one-parameter fits.

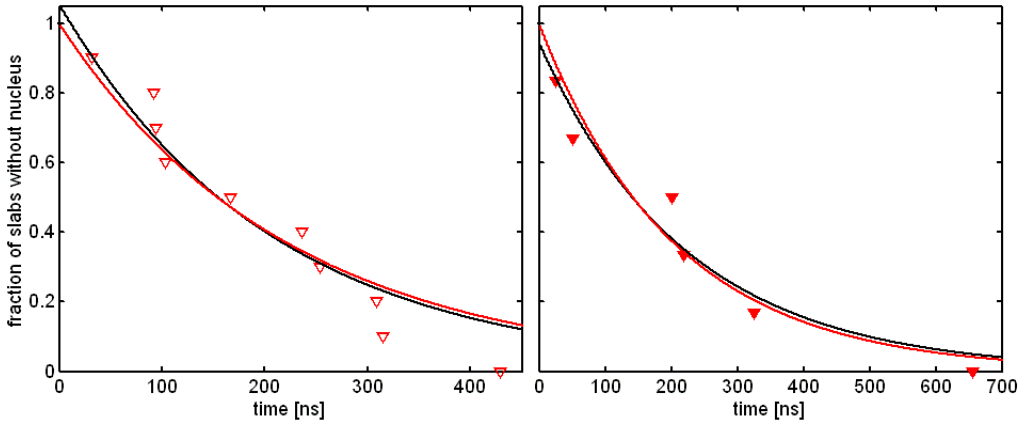

Figure 5.7. Fraction of slabs of water covered by pentanoic acid without an ice nucleus plotted against time separately for subsurface and bulk nucleation. The left part corresponds to the subsurface nucleation, the right part to the bulk one. Black and red curves represent two-parameter and one-parameter fits.

Table 5.2. Nucleation times for all slabs of water covered by pentanoic acid and for subsurface and bulk nucleation separately in ns.

	all	subsurface	bulk
1-parameter fit	231	222	205
2-parameter fit	220	207	222

Results for one-parameter and two-parameter fit differ by less than 20 ns, the most pronounced difference occuring for separate bulk nucleation. One-parameter fit again predicts shorter nucleation times for both separate cases that for the total one, which cannot be correct. Bulk and subsurface nucleation seem to scale similarly. The nucleation time in the water slab covered by pentanoic acid probably lies between 215-235 ns, which is in the same range as that for neat water, i.e. 220-230 ns. The pentanoic acid coverage does not change the kinetics of homogenenous ice nucleation, it just slightly decreases the subsurface preference.

Finally, I have examined the effect of pentanol on the onset of freezing, as depicted in Figures 5.8 and 5.9. Empty blue squares refer to the subsurface nucleation, while filled symbols to the bulk one. Nucleation events were observed in 29 water slabs covered by this surfactant, 14 of them occurred in the bulk, so it seems that there is no preference for subsurface nucleation.

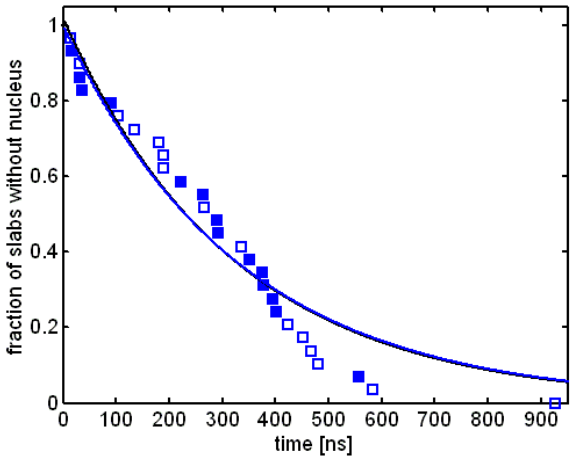

Figure 5.8. Fraction of slabs of water covered by pentanol without an ice nucleus plotted against time. Empty blue squares correspond to a nucleus created in the subsurface, while filled squares represent a nucleus formed in the bulk region. Black and blue curves represent two-parameter and one-parameter fits.

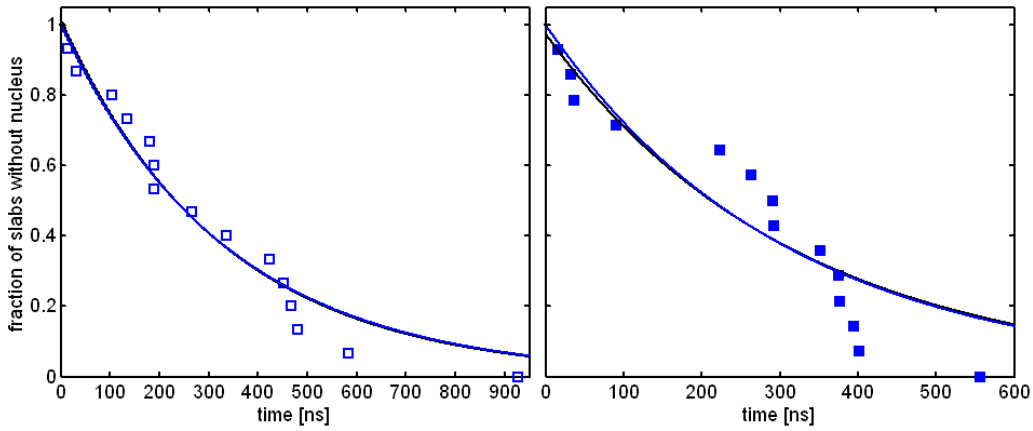

Figure 5.9. Fraction of slabs of water covered by pentanol without an ice nucleus plotted against time separately for subsurface and bulk nucleation. The left part corresponds to the subsurface nucleation, the right part to the bulk one. Black and blue curves represent two-parameter and one-parameter fits.

Data were separated and fitted similarly as for the previous systems. Black and blue curves represent two- and one- parameter fits, respectively; the corresponding nucleation times are provided in Table 5.3. One-parameter and two-parameter fits differ by less than 10 ns, the most pronounced difference is in the case of separate bulk nucleation. The nucleation time for water slab covered by pentanol is about 50% longer than in previous two cases, i.e. about 330 ns. Extracted characteristic times for bulk nucleation are slightly lower than for subsurface one, but the difference is negligible. To conclude, pentanol decreases subsurface preference and prolongs nucleation time in water slab.

Table 5.3. Nucleation times for all slabs of water covered by pentanol and for subsurface and bulk nucleation separately in ns.

	all	subsurface	bulk
1-parameter fit	333	336	309
2-parameter fit	325	330	319

Non of the systems exhibit perfectly exponential decay, and separation of subsurface and bulk values did not improve the situation. In an ideal case, we should obtain the same characteristic times for bulk nucleation in all three systems, but we did not. Probably due to the finite system size the bulk region is still influenced by the interfaces. Finally, to clearly demonstrate, that ice nucleation is slower in water covered by pentanol, there is a Figure 5.10, that contains all nucleation events observed in this work.

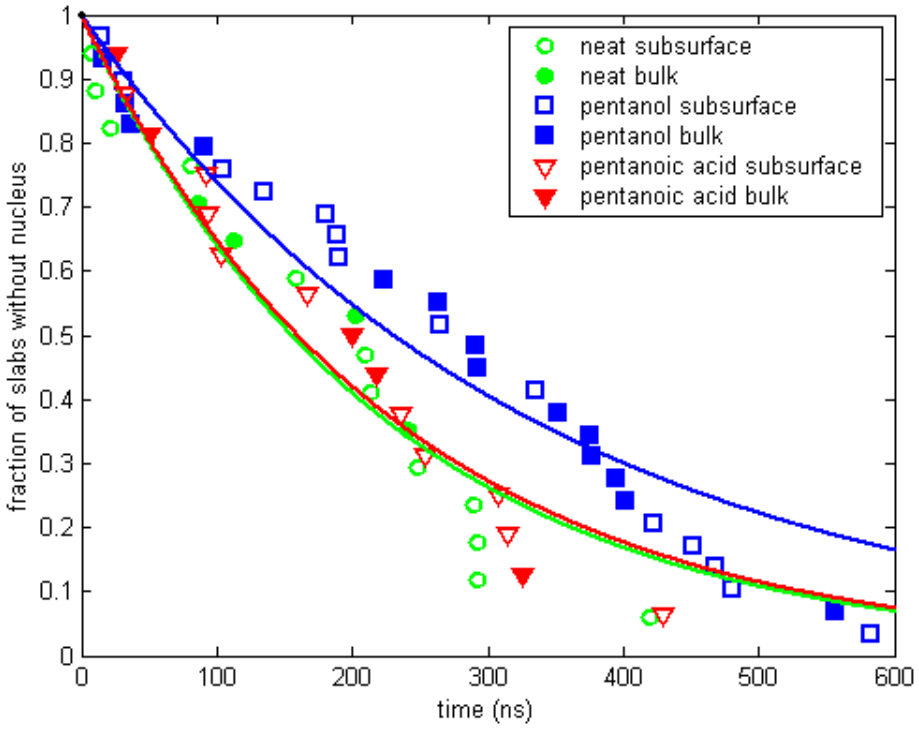

Figure 5.10. Fraction of slabs without an ice nucleus plotted against time. Empty symbols represent a nucleus created in the subsurface, while filled symbols refer to a nucleus formed in the bulk region. Green circles correspond to neat water, red triangles to water covered by pentanoic acid, and blue squares to water covered by pentanol.

5.3 Interpretation of the effect of adsorbates

Pentanol influences the formation of ice more than pentanoic acid, it slows down nucleation rate and subsurface preference. Why is it so? This section tries to answer this question. The first idea was, that the acid molecules interact more likely with other acids than with waters, because the interaction energy of acid homodimer is larger than that of acid-water heterodimer. Therefore, water molecules in the surface layer would be less affected. This would not be the case for pentanol, because interaction energies of possible pairs are much closer to each other. To check this hypothesis, I have calculated the average number of hydrogen bonds between water and adsorbate molecules. Note, that pentanoic acid can also act as hydrogen acceptor at carbonyl oxygen. One pentanoic acid molecule forms 2.3 hydrogen bonds with water and 0.2 hydrogen bonds with another acid, while pentanol forms 2.3 hydrogen bonds with water and 0.15 hydrogen bonds with another alcohol. Although the interaction energies of water-adsorbate and adsorbate-adsorbate pair are different in both systems, number of hydrogen bonds formed between them is comparable and does not help with the explanation of the different behaviour of the adsorbates.

Therefore, I looked more closely at orientation of water molecules across the slab of water. This means plotting the probability of finding a water molecule at a given z position with certain orientation of the dipole with respect to the z-axis. This is the axis perpendicular to the air/water or adsorbate/water interface. The corresponding angle is depicted in Figure 5.11.

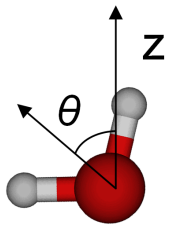

Figure 5.11. Orientation of water dipole with respect to the z-axis.

At first, I analysed the supercooled liquid water in all three investigated systems. Results are shown in Figure 5.12, where brighter areas correspond to higher probability and darker areas to lower probability. Except for the surface area, the orientation of water molecules is random and, therefore, the color of the corresponding area is uniform. The situation is different at the interface. In case of neat water (Figure 5.12 a)), there is an enhanced probability of the value $\cos\theta$ close to zero, which means,

that one hydrogen is pointing out from the liquid. In surface contaminated systems (Figure 5.12 b) for pentanoic acid and Figure 5.12 c) for pentanol), there is an enhanced probability $\cos\theta$ having negative values at the upper interface and positive values at the lower interface, which is indication that oxygens are pointing towards the adsorbates. Pentanoic acid orients interfacial water molecules more strongly than pentanol, as can be seen from brighter color in the above mentioned regions.

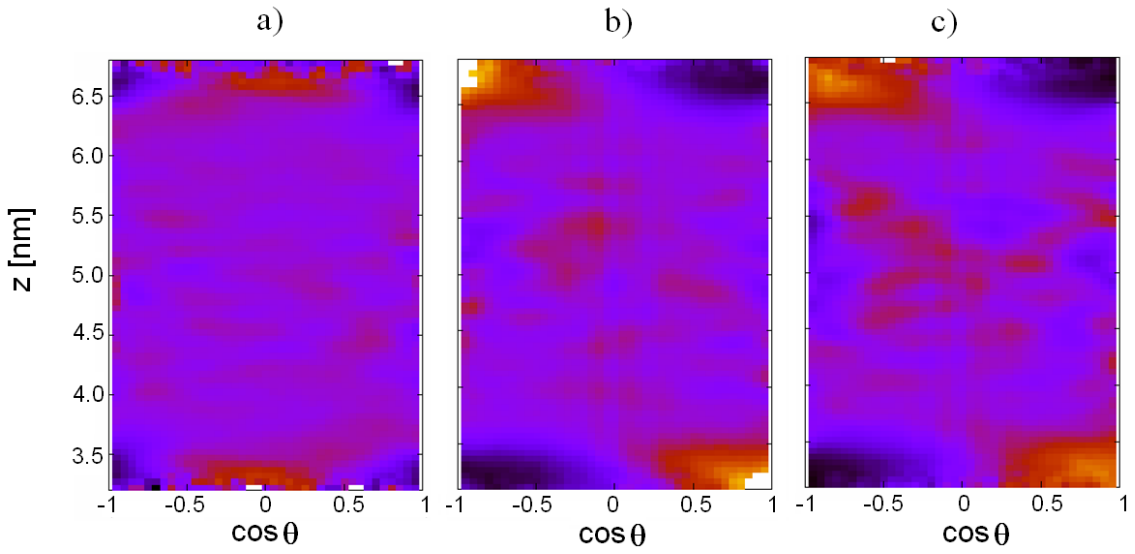

Figure 5.12. Orientation maps of dipoles of water molecules in supercooled liquid in neat water a), water covered by pentanoic acid b), and water covered by pentanol c). Colour coding corresponds to probability distribution as a function of z-coordinate and $\cos\theta$ defined in Figure 5.11. Brighter color means a more probable orientation.

Orientation maps of selected frozen systems with corresponding snapshots are presented in Figure 5.13. The orientation of water molecules at the interface did not change, because they remain unfrozen. But certain orientations of water molecules are enhanced (brighter areas) and certain suppressed (darker areas) in crystalline ice. The most significant difference can be seen in case of water covered by pentanoic acid (Figure 5.13 b)), because the basal plane of ice is perpendicular to the z-axis, as indicated by the dashed blue line. Basal plane in other two systems are tilted with respect to the z-axis, that is why the obtained picture is not so clear. If we choose a direction perpendicular to the basal plane for mapping, we will get the same picture as for water covered by pentanoic acid. Ice formed in the selected neat water slab (Figure 5.13 a)) seems to be more disordered than that formed in (Figure 5.13 c)).

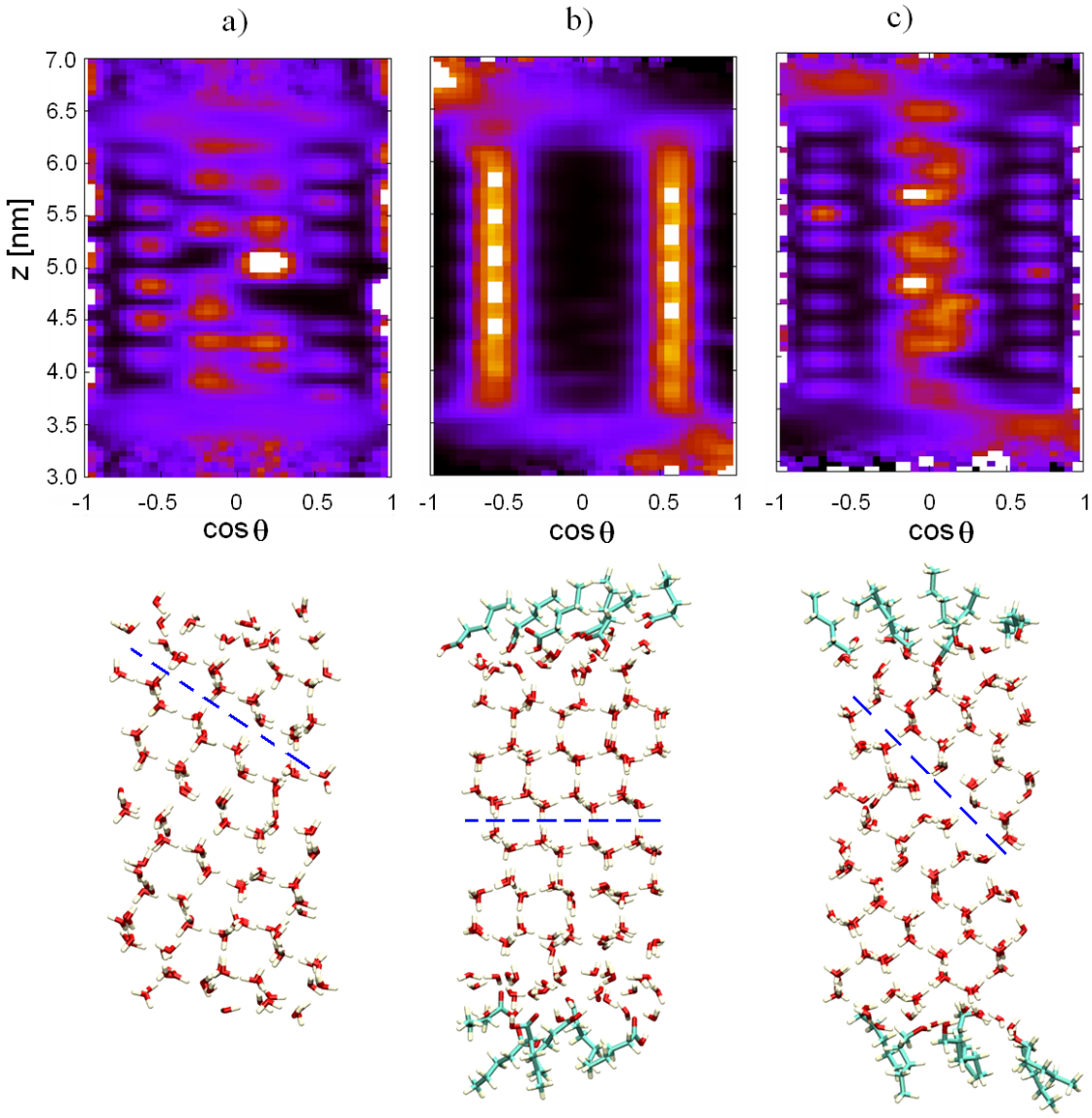

Figure 5.13. Orientation maps of dipoles of water molecules in selected frozen systems with corresponding snapshots: neat water a), water covered with pentanoic acid b), and water covered with pentanol c). Colour coding in orientation maps corresponds to probability distribution as a function of z-coordinate and $\cos\theta$ defined in Figure 5.11. Brighter color means a more probable orientation. Dashed blue line indicates the direction of the basal plane.

Note, that the investigated systems do not significantly differ from each other in the crystal structure of the formed ice. Homogeneous nucleation typically leads to formation of a mixture of cubic and hexagonal ice, while only rarely pure cubic or pure hexagonal ice is formed. This is in agreement with conclusions of other investigators [36] who observed formation of hexagonal ice on a cubic substrate and vice versa even several times during crystallization. From averaging over trajectories, it was found that systems differ in orientation of basal plane with respect to the interface. This plane is mainly tilted in the case of neat water, both tilted and coplanar in case of water covered by pentanol, and mainly coplanar in case of water covered by pentanoic acid. Pentanoic acid orients strongly not only interfacial water molecules, but also the ice planes. The effect of pentanoic acid on both observables is stronger than that of alcohol. Up to now, this is in contradiction with small influence of the coverage of the acid on the onset of freezing, but note that only structural properties have been discussed, no "dynamics" has been presented yet.

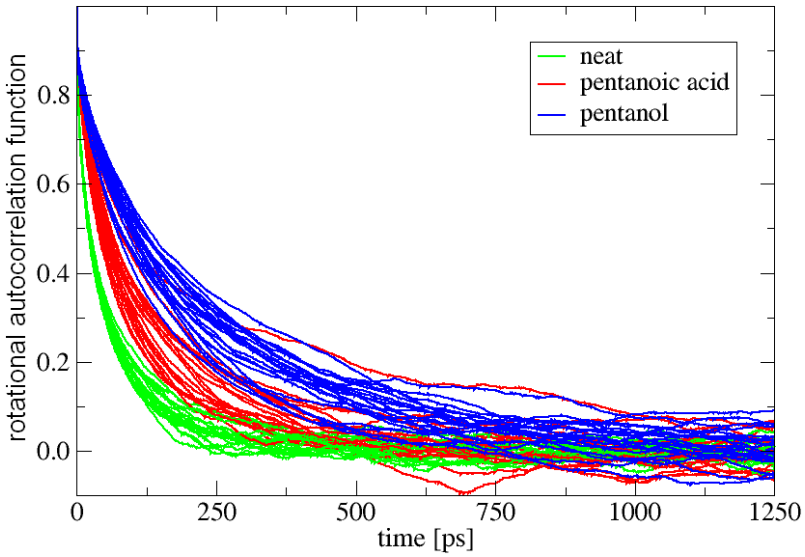

Figure 5.14. Average rotational autocorrelation functions of 8 most interfacial water molecules in neat water (green), water covered by pentanoic acid (red), and water covered by pentanol (blue). The correlation functions were evaluated every 5 ns for the first 100 ns of the trajectory. Each line corresponds to one evaluation.

The mobility of water molecules at the interface is important for homogeneous ice nucleation in the subsurface, since it helps to accommodate changes in the local structure and increase of volume during freezing. The rotational autocorrelation function was used to represent mobility of interfacial water molecules. Figure 5.14

shows the average rotational autocorrelation function of 8 most interfacial water molecules in all three investigated systems. In case of neat water correlation time is the shortest, while for water molecules in contact with pentanol, it is the longest.

On one hand the mobility of interfacial water molecules represents a kinetic advantage for homogeneous ice nucleation, on the other hand forcing water molecules into certain orientations also helps nucleation, since films of long-chain surface active substance are efficient nucleators. Taking all these things together, the following conclusion can be drawn. Adsorbates have an orientation effect, as demonstrated by orientation of water molecules at the interface and orientation of ice planes. At the same time, they also hinder the motion of interfacial water molecules which slows down nucleation. These effects practically compensate in case of pentanoic acid, which has almost the same kinetics for ice nucleation as neat water (with slightly decreased subsurface preference) but for different reason. For pentanol, hindering is stronger causing no subsurface preference and nucleation time, which is longer than in neat water.

5.4 Final remarks

Homogeneous freezing observed in MD simulations starting from both bulk and subsurface regions is not just a special feature of the NE6 model. In our group, we have produced a nucleation trajectory employing the TIP5P model [56] at 240 K, which lies 35 K below its melting point, and also one nucleation trajectory using the TIP4P/2005 water model [54] at 210 K, which is about 40 K below its melting point.

The system for which the majority of simulations was performed is small, therefore, a relatively small cut off was used. Consequently, important questions about size effects and artificial periodicity arise. Increasing the size of the system in the z-direction has been discussed in this chapter. I have also considered increasing the size of the system in x and y directions, but have not obtained a single nucleation trajectory after hundreds of ns. Nucleation is a stochastic event, therefore it is not surprising that it was not observed in a single trajectory of a finite length for the larger system. Also nucleation in the systems with small lateral dimensions might be speeded up by artificial periodicity. This should not, however, affect difference between three investigated systems, since they would be affected in the same way. Also, Vega and coworkers reported, that size of the system does not play a significant role for melting [68].

Chapter 6

Conclusion and outlook

Homogeneous ice nucleation in neat and surface contaminated water has been studied by means of extensive molecular dynamics simulations. Freezing preferentially starts in the subsurface of neat water and water covered by pentanoic acid, where this preference is slightly decreased. Nucleation time in these systems is about 220-230 ns. Pentanol surface pollution increases the nucleation time by 50% and washes out the subsurface preference. Based on analysis of MD trajectories, it seems that the same kinetics in the first two cases has different reason. The surfactants orient water molecules, which enhances nucleation, but also decrease the mobility of interfacial water molecules, which at the same time slows down nucleation. The latter effect is stronger in case of pentanol, therefore slabs covered by it exhibit no subsurface preference. In contrast, both effects are comparable in case of pentanoic acid, where ice with its coverage has planes mostly oriented coplanar with respect to the interface. From the perspective of atmospheric processes it is interesting, that different pollutants have different effects.

Short chain alcohols are known as anti-freeze agents, while Langmuir monolayers of long chain aliphatic alcohols are efficient ice nucleators. The disordered layer of pentanol, employed in this work, is an intermediate case. It would be beneficial to study the effect of different coverage of the surface, as well as the effect of the chain length on homogeneous ice nucleation. The influence of other pollutants, such as aldehydes may be also interesting. Water does not occur in nature as a pure species, but it dissolves many compounds such as salts. One nucleation trajectory of NaCl solution has already been produced [23], but information about the influence of other salts like ammonium sulphate would be important for the atmospheric community. Hopefully, future simulation studies will address these questions.

Appendix A

List of abbreviations

AIN	atmospheric ice nucleus
FF	force field
IN	ice nucleus
MD	molecular dynamics
LJ	Lennard-Jones
MP2	Møller-Plesset perturbation theory of the second order
NE6	six-site water model
PBC	periodic boundary conditions
PES	potential energy surface
TIP4P	four-site water model
TIP5P	five-site water model
vdW	van der Waals

Appendix B

Force field parameters

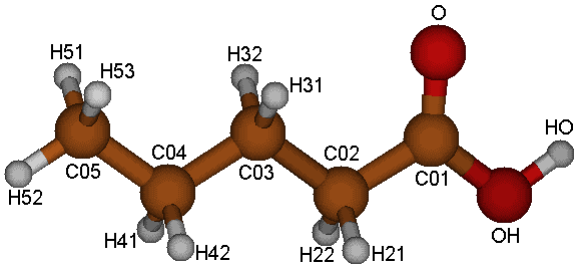

Figure B.1. Pentanoic acid with labelled atom types.

Table B.1. Intermolecular forcefield parameters of pentanoic acid based on Amber parm99 [59] and RESP charge fitting.

Name	Atom type	Partial charge [e]	σ [nm]	ϵ [kJ·mol^{-1}]
HO	HO	0.438	0.000	0.000
OH	OH	-0.643	0.307	0.880
O	O	-0.608	0.296	0.879
C01	C	0.737	0.340	0.360
C02	CT	-0.091	0.340	0.458
C03	CT	-0.021	0.340	0.458
C04	CT	0.018	0.340	0.458
C05	CT	-0.086	0.340	0.458
H21	HC	0.058	0.265	0.066
H22	HC	0.058	0.265	0.066
H31	HC	0.032	0.265	0.066
H32	HC	0.032	0.265	0.066
H41	HC	0.005	0.265	0.066
H42	HC	0.005	0.265	0.066
H51	HC	0.022	0.265	0.066
H52	HC	0.022	0.265	0.066
H53	HC	0.022	0.265	0.066

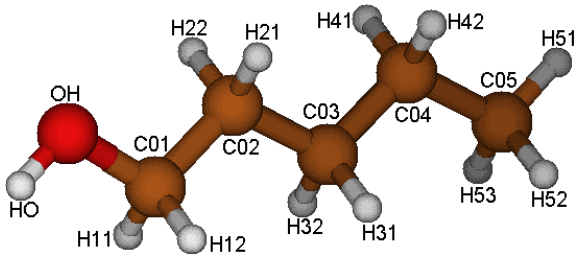

Figure B.2. Pentanol with atoms labelled in the same way as in Tables B.2 and B.3.

Table B.2. Intermolecular forcefield parameters of pentanol based on Amber parm99 [59] and RESP charge fitting.

Name	Atom type	Partial charge [e]	σ [nm]	ϵ [kJ·mol^{-1}]
HO	HO	0.433	0.000	0.000
OH	OH	-0.701	0.307	0.880
C01	CT	0.231	0.340	0.458
C02	CT	-0.003	0.340	0.458
C03	CT	-0.004	0.340	0.458
C04	CT	0.038	0.340	0.458
C05	CT	-0.046	0.340	0.458
H11	H1	-0.006	0.247	0.066
H12	H1	-0.006	0.247	0.066
H21	HC	0.035	0.265	0.066
H22	HC	0.035	0.265	0.066
H31	HC	0.006	0.265	0.066
H32	HC	0.006	0.265	0.066
H41	HC	-0.006	0.265	0.066
H42	HC	-0.006	0.265	0.066
H51	HC	0.009	0.265	0.066
H52	HC	0.009	0.265	0.066
H53	HC	0.009	0.265	0.066

Table B.3. Modified intermolecular forcefield parameters of pentanol.

Name	Atom type	Partial charge [e]	σ [nm]	ϵ [kJ·mol^{-1}]
HO	HO	0.393	0.000	0.000
OH	OH	-0.705	0.307	0.880
C01	CT	0.231	0.340	0.558
C02	CT	-0.003	0.340	0.558
C03	CT	-0.004	0.340	0.558
C04	CT	0.038	0.340	0.558
C05	CT	-0.046	0.340	0.558
H11	H1	-0.002	0.247	0.077
H12	H1	-0.002	0.247	0.077
H21	HC	0.039	0.265	0.077
H22	HC	0.039	0.265	0.077
H31	HC	0.010	0.265	0.077
H32	HC	0.010	0.265	0.077
H41	HC	-0.002	0.265	0.077
H42	HC	-0.002	0.265	0.077
H51	HC	0.013	0.265	0.077
H52	HC	0.013	0.265	0.077
H53	HC	0.013	0.265	0.077

Appendix C

Publication

Pluhařová, E.; Vrbka, L.; Jungwirth, P. *J. Phys. Chem. C* **2010** (in press)

Effect of Surface Pollution on Homogeneous Ice Nucleation: A Molecular Dynamics Study

Eva Pluhařová,*,† Luboš Vrbka,‡ and Pavel Jungwirth†

Institute of Organic Chemistry and Biochemistry, Academy of Sciences of the Czech Republic, and Center for Complex Molecular Systems and Biomolecules, Flemingovo nám. 2, 16610 Prague 6, Czech Republic, and Institute of Physical and Theoretical Chemistry, University of Regensburg, Universitätstraβe 31, 93040 Regensburg, Germany

Received: September 18, 2009; Revised Manuscript Received: January 18, 2010

Homogeneous ice nucleation in neat and surface contaminated water has been studied by means of molecular dynamics simulations. In neat water, nucleation preferentially starts in the subsurface region, which accommodates better than the bulk the volume increase associated with freezing. As models of the adsorbates, we have assumed pentanol and pentanoic acid. Homogeneous ice nucleation is affected more by alcohol than by acid. Water slabs covered by a disordered layer of pentanol exhibit negligible preference for subsurface nucleation and longer nucleation times in comparison with neat water, while nucleation times are almost unaffected by the presence of pentanoic acid and the subsurface preference is only slightly decreased. The effect of adsorbates has important implications for the microphysics of formation of high altitude clouds upon conditions when a wide range of high molecular weight compounds are emitted to the atmosphere during biomass burning.

Introduction

Homogeneous ice nucleation has been shown to be crucial for the microphysics of formation of high altitude cirrus clouds and polar stratospheric clouds, as well as for glaciation of thunderclouds.[1−4] There is an ongoing discussion whether homogeneous freezing starts preferentially in the aqueous bulk or at the surface of the droplets.[5−8] If the surface or subsurface is relevant for nucleation, as is likely in particular in the case of small droplets, then pollution can be very important. However, the effects of organics on the ice nucleation behavior of upper tropospheric aerosols are not very well understood.[9] On one hand, some laboratory studies have indicated that homogeneous freezing of low molecular weight carboxylic acids solutions is not as efficient as in aqueous sulfate aerosols, with others having found practically unaffected nucleation efficiencies.[10,11] On the other hand, certain inorganic and organic substances were shown to possess the ability to enhance ice nucleation.[12] Amphiphilic molecules forming Langmuir monolayer films may be designed such that their hydrophilic head groups create a surface template for the future nucleated ice crystal. For example, induced freezing of drops of supercooled water covered by ordered monolayers of long chain (i.e., with more than 10 CH_2 groups) aliphatic alcohols and carboxylic acids was extensively studied both experimentally[13−20] and theoretically.[21,22] The ice-nucleation temperatures were found to depend on the length of the hydrocarbon chain and the even−odd parity of carbon atoms, as well as on the chemical nature of the head group. A systematic increase in nucleation temperature was found for long chain alcohols (but not carboxylic acids) starting from about 15 carbon atoms.[13]

Ice nucleation and freezing of aqueous droplets can be monitored experimentally or with the use of computer simulations. Measurements on supercooled water are difficult to perform because of the high probability of uncontrolled ice nucleation in samples of normal size and purity.[23] Several approaches exist for experimental investigation of freezing of smaller water droplets in the micrometer and even nanometer size range, such as those employing electrodynamic Paul-traps,[24] free-fall tubes,[25] emulsified droplets,[26] and jet expansions.[27] High-speed monitoring of the freezing process of freely suspended supercooled pure and salty water droplets has been reported for the first time employing the method of acoustic levitation combined with IR/VIS high-speed imagining.[28] These experiments show that nucleation starts preferentially in the interfacial region, which is in agreement with a previous study.[8] However, laboratory measurements employing the method of electrodynamical levitation indicate that homogeneous ice freezing is a volume-proportional process with surface nucleation being potentially important for small droplets with radii below 20 μm.[6] Volume nucleation is more probable for bigger droplets simply because many more molecules are present in the bulk than in the surface layer. It was also found that in some emulsion experiments the presence of surfactants at the oil/water interface prevents surface nucleation.[5] In these cases, volume nucleation is the favored nucleation process. These authors further proposed that for droplets in air surface nucleation is, nevertheless, the preferred nucleation process. At the moment, neither surface nor volume dependent nucleation processes are unequivocally supported by measurements. The analysis remains inconclusive, since the scatter in experimental data from various techniques is too large.[7]

There exist only a handful of computational studies of homogeneous ice nucleation. The first successful study was performed using the TIP4P water model,[29] the melting point of which is 232 K, and only a single nucleation trajectory was obtained.[30] Soon thereafter, a six-site water potential abbreviated as NE6[31] for simulation of ice and water near the experimental

* To whom correspondence should be addressed. E-mail eva.pluharova@uochb.cas.cz.

† Institute of Organic Chemistry and Biochemistry, Academy of Sciences of the Czech Republic, and Center for Complex Molecular Systems and Biomolecules.

‡ University of Regensburg.

10.1021/jp9090238

melting point was developed. Employing this model, ice growth from supercooled water in contact with crystalline of ice was simulated at conditions close to experimental reality.[32−34] Using the NE6 model, we were able to show that in slabs of varying sizes homogeneous ice nucleation starts preferentially in the subsurface.[35] In that study, we also produced the first freezing trajectory employing the TIP5P model.[36] Recently, we succeeded in simulating homogeneous ice nucleation and brine rejection in a salt solution, again using the NE6 water model.[28]

In the present study, we aim at answering the following questions. How do surface active substances affect homogeneous ice nucleation in water? Does nucleation occur preferentially in the subsurface or in the bulk of polluted water? How do adsorbates influence the time required for the formation of the ice nucleus? What is the effect of different head groups of the surface active species?

Pentanoic acid and pentanol serve as model compounds for organic acids and alcohols present in atmospheric aerosols. Monocarboxylic acids (C6−C34) have been observed in field measurements,[37] long-chain alcohols and fatty acids have been mentioned in ref 38, and alcanoic acids (C10−C32) and alcanols (C10−C34) in refs 39 and 40. The investigated adsorbates are small enough to make the nucleation simulation feasible, but their aliphatic chains are at the same time long enough to ensure sufficiently low solubility in water. The maximal mole fraction of pentanoic acid in a binary mixture with water at 298.15 K is 0.0065,[41] and a saturated water−pentanol mixture at 293.15 K contains 0.0049 of pentanol.[42] Extending our previous studies,[28,35] we have simulated homogeneous ice nucleation in slabs containing either neat water or water covered by a disordered layer of adsorbate. Nucleation is a stochastic event, the description of which requires more than a single trajectory for each system. We thus base our conclusions on a set of more than 60 successful nucleation trajectories.

Systems and Force Fields

Molecular dynamics (MD) simulations of homogeneous freezing of aqueous slabs were performed using a six-site interaction potential for water NE6.[31] This potential was optimized for simulations of water and ice near the experimental melting point T_m. Only few models yield satisfactory values of T_m, such as TIP4P/Ice[43] and TIP5P.[36] The former model also provides a good description of the phase diagram involving solid phases, while TIP5P fails for this purpose.[44] A first report of T_m for the NE6 was very close to the experiment. In a recent paper, the authors refined the melting point to the range 280−285 K.[45] Two different methods were used for the calculation of T_m for the NE6 potential. The first one is a combination of a Gibbs−Duhem integration and free energy calculations, and the second one a determination of the melting temperature by direct coexistence. In summary, averaging the results obtained with both methods, 289 K is proposed as the most likely value of T_m.[44] The new estimate thus places the melting temperature about 16 degrees above the experimental value. For the purpose of the present study, this is an acceptable deviation which has, moreover, the advantage of yielding somewhat faster crystallization rates.[33]

Pentanol and pentanoic acid were adopted as model surface adsorbates. Geometry and charge distribution of adsorbate molecules were taken from ab initio calculations at the MP2/aug-cc-pVDZ level of theory. Other force field parameters were adopted from AMBER parm99.[46] Interaction energies of pairs water−adsorbate, adsorbate−adsorbate, and water−water were compared with MP2/aug-cc-pVDZ results. Optimized structures of mentioned pairs are depicted in Figure 1. The NE6 water model employed here somewhat overestimates the interaction energy of the water dimer, which is the prize for achieving good bulk properties with a nonpolarizable model. In the pentanol−water pair (Figure 1d), water should be a better hydrogen bond donor than pentanol according to ab initio calculations. Reversed ordering of hydrogen bonding strength in the alcohol−water pair resulting from empirical force field has been noticed previously.[22] In order to fix this, partial charges and Lennard−Jones parameters on pentanol atoms were slightly modified in order to achieve the correct ordering of hydrogen-bonding strength. Parameters for pentanoic acid give satisfactory results, and therefore, no adjustment was necessary here. Force-field parameters for the employed adsorbate molecules are summarized in Table 1, while Table 2 reports on comparison with MP2 calculations.

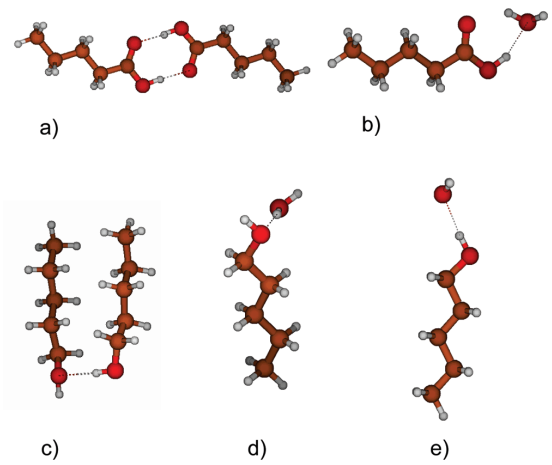

Figure 1. Optimized geometries (at the MP2/aug-cc-pVDZ level) of pentanoic acid dimer (a), pentanoic acid−water complex (b), pentanol dimer (c), and pentanol−water complexes (d, e).

TABLE 1: Intermolecular Potential Parameters Employed in This Study

molecule	atom type	charge	σ [nm]	ε [kJ/mol]
pentanol	HO	0.393	0.00	0.00
	OH	−0.705	0.307	0.880
	CT	0.231	0.340	0.558
	H1	−0.0025	0.247	0.076
	HC	0.039	0.265	0.076
pentanoic acid	O	−0.608	0.296	0.879
	OH	−0.643	0.307	0.880
	HO	0.438	0.00	0.00

TABLE 2: Comparison of Force Field Interaction Energies with Ab Initio Calculations at the MP2/aug-cc-pVDZ Level for Structures from Figure 1[a]

	structure				
	a	b	c	d	e
MP2	71.5	39.5	32.2	23.5	18.3
AMBER parm99[46]	68.4	41.7	30.8	26.3	28.9
modified			30.4	26.8	21.8

[a] Energies in kJ/mol.

Simulation Methods

The simulated aqueous systems were placed in a rectangular prismatic box extended in the z-direction, and 3D periodic

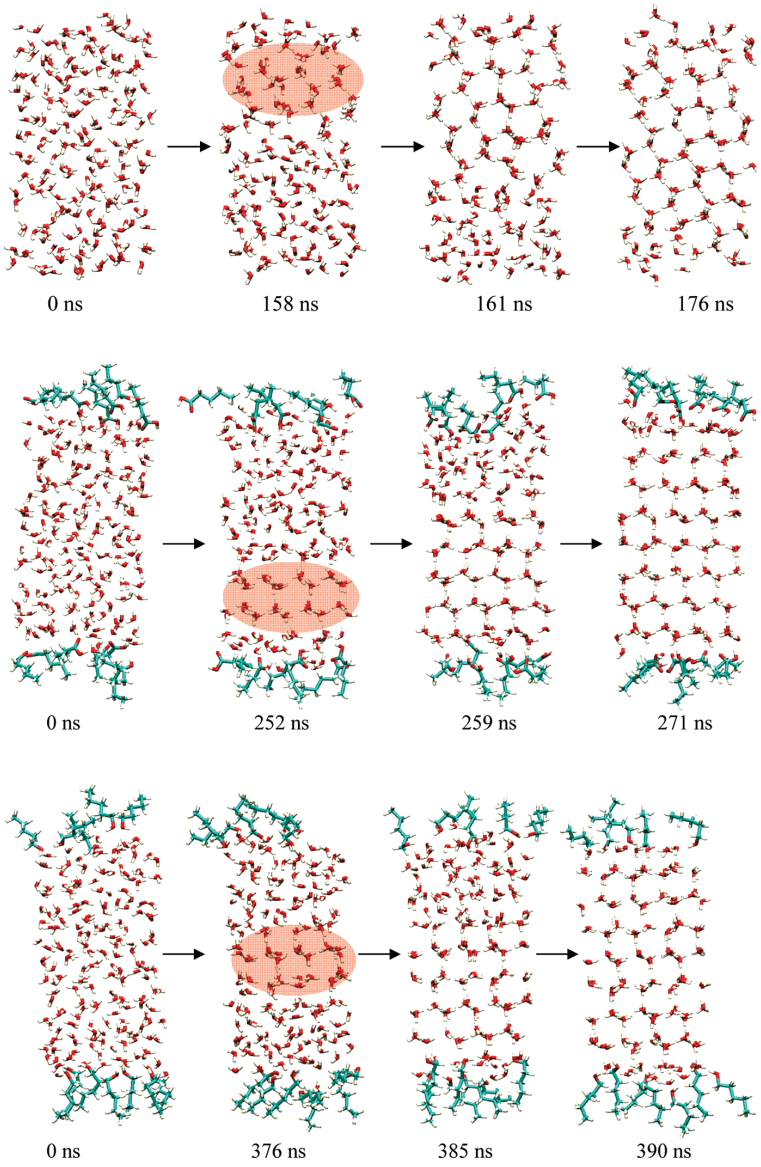

Figure 2. Four snapshots from a selected nucleation trajectory for each system under study: neat water (top), water covered by pentanoic acid (middle), and water covered by pentanol (bottom). Only the unit cell, containing 192 water molecules and possibly the 12 adsorbate molecules, is depicted. The shaded regions highlight the newly formed ice nucleus. In the depicted cases, nucleus was formed in the subsurface region for neat water after ~160 ns. In water covered by pentanoic acid it also formed in the subsurface after ~250 ns, while in water covered by pentanol it took ~380 ns to form a nucleus close to the center of the slab.

boundary conditions were applied. This resulted in the formation of an infinite slab (more precisely, an infinite series of practically noninteracting slabs) with a bulk region in between two surfaces in the *xy*-plane. The smallest unit cells with approximate dimensions 13.5 × 15.5 × 100 Å^3 contained 192 water molecules. First, a unit cell with dimensions of 13.5 × 15.5 × 29.5 Å^3 was chosen such as to correspond to a rectangular cell of ice Ih, and subsequently, the *z*-dimension was extended to 100 Å^3. This size is just large enough to provide the slab with a well developed bulklike region,[47,48] but small enough to allow for extremely long simulations needed for capturing homogeneous nucleation in water. Larger slabs used for test calculations were constructed by doubling or tripling the width of the original cell, yielding systems with 384 or 576 water molecules in the unit cell. The *z*-dimension was consequently prolonged to 180 or 270 Å, respectively. Surface contaminated water slabs were constructed by adding six pentanol or pentanoic acid molecules on each of the two surfaces, forming an incomplete and disordered layer.

Long range electrostatic interactions were accounted for using the smooth particle mesh Ewald method, employing a pseudo-2D correction for the slab geometry.[49] Nonbonded interactions had to be cut off at a relatively short distance of 6.5 Å due to the small size of the simulation cells in the *x*- and *y*-dimensions.

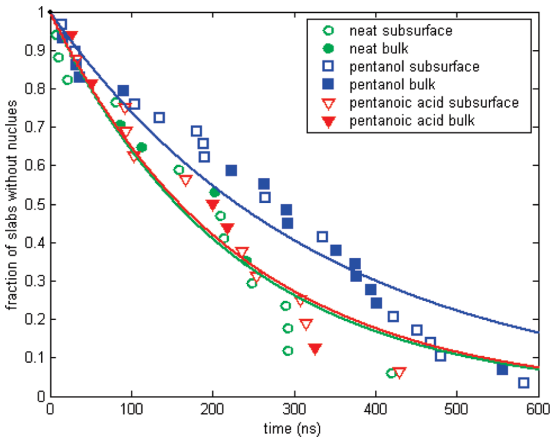

Figure 3. Fraction of slabs without an ice nucleus plotted against time. Empty symbols correspond to a nucleus created in the subsurface, while filled symbols represent a nucleus formed in the bulk region. Green circles correspond to neat water, red triangles to water covered by pentanoic acid, and blue squares to water covered by pentanol.

After preparation of the liquid water systems and short pre-equilibration period at a given temperature, the production runs followed. Newton equations of motion were propagated with a time step of 1 fs for 100−1800 ns (depending on the occurrence of a nucleation event in a given trajectory).

To avoid possible problems with the quantum nature of OH vibrations, we used the LINCS algorithm to constrain bonds involving hydrogen atoms.[50] This makes the calculations computationally more efficient and also leads to faster equilibration and thermalization of the unconstrained degrees of freedom. OH vibrations do not play a very important role in freezing process, because ice growth occurs at much longer time scales than OH vibrations do. The slower translational and rotational/librational motions are, therefore, more relevant. Temperature was adjusted using the Nose-Hoover thermostat.[51] The optimal freezing temperature and temperature coupling constant were determined in our previous work.[35] The fastest ice nucleation occurred at the temperature of 250 K, maintained using a temperature coupling constant of 0.5 ps. For each system, we carried out about 20 simulations for the smallest cell, with an additional two runs for the two larger cells, all with different starting coordinates for each run. All calculations were performed using the GROMACS 3.3 program package.[52]

Results

The main goal of this work was to explore the differences in homogeneous ice nucleation in neat and surface contaminated water and compare these in terms of the preferred spatial location of nucleus and the time required for its formation. Homogeneous ice nucleation is a rare event, the simulation of which is extremely time-consuming. Moreover, the stochastic character of this process requires a large number of simulation trajectories in order to provide statistically meaningful results. Therefore, we have performed tens of simulations only for the smallest slabs which, however, already have a well developed bulk region in between the two interfaces.[47,48] There is an important issue of possible size effects on the results. We have also obtained several nucleation trajectories for slabs containing 384 and 576 water molecules, yielding qualitatively similar results. Increasing the size of the system in the *z*-direction does not change the nucleation process significantly, as shown also in our previous studies.[35] We also considered increasing the size of the system in the lateral dimension by duplicating in both the *x*- and *y*-direction. However, this quadruples the size of the system, making the simulations more than an order of magnitude slower; therefore, we were not able to collect a long enough trajectory to resolve the issue. For now, we can at least state that for the reverse (and computationally simpler) process of ice melting size effects do not play a big role. This has been satisfactorily addressed by Vega and co-workers who reported that coexistence of water and ice and melting temperature are not affected within the statistical error by system size.[53]

Figure 2 shows four snapshots from one successful nucleation trajectory for each system under study: neat water (top), water covered by pentanoic acid (middle), and water covered by pentanol (bottom). Only the unit cell, containing 192 water molecules and, in the latter two cases, also the 12 adsorbate molecules, is depicted. The shaded regions highlight the newly formed ice nucleus. In the selected trajectory for neat water, the nucleus was formed in the subsurface region, which is in accord with our previous study,[35] after ∼160 ns. In water covered by pentanoic acid, it also formed in the subsurface after ∼250 ns, while in water covered by pentanol it took ∼380 ns to form a nucleus close to the center of the slab. We should stress here that this figure serves just as an illustration and we base our further conclusions on an ensemble of tens of nucleation events for each system.

The onset of crystallization can be monitored in several ways: (1) observing formation of six-membered rings as can be seen from snapshots; (2) searching for "long lasting" hydrogen bonds between four-coordinated water molecules; "long lasting" means having a lifetime more than 2 ns; (3) potential energy decreases during the freezing period, so the beginning of this decrease indicates nucleation; (4) plotting evolution of the density profile in time. The last approach was presented in ref 54, while the previous two were suggested by Matsumoto et al.[30] All four approaches were tested in the present study, and the corresponding nucleation times differ by less than 2 ns. For further discussion, we used the first approach.

The main results of this work are shown in Figure 3 which displays the fraction of slabs without an ice nucleus formed plotted against time. Our statistics is based on 17 nucleation trajectories for neat water, 29 for water contaminated by pentanol, and 16 for water contaminated by pentanoic acid. Every symbol in the figure represents formation of a stable ice nucleus at a given time. Empty symbols correspond to a nucleus created in the subsurface, while filled symbols represent a nucleus formed in the bulk region. Nucleation preferentially starts in the subsurface in neat water (subsurface to bulk ratio of 12:5) and in water covered by acid (subsurface to bulk ratio of 10:6) with the subsurface preference slightly decreased in the latter case. There is, however, virtually no preference for subsurface nucleation for water contaminated by alcohol (subsurface to bulk ratio of 15:14). Note that by "surface" we mean the first layer (3−4 Å thick); it does not necessarily have to be the "surface" as assumed by Tabazadeh and co-workers[5] in macroscopic experiments, with their scale being different. The vapor−liquid interface of water has been studied, for example, in refs 47 and 48; mainly based on analysis of the hydrogen bond network (calculating hydrogen-bonded neighbors), it was concluded that the shortest distance from the aqueous liquid−vapor interface at which one can observe bulk liquid behavior is approximately 10 Å. Using this result, our system has a 10−12 Å thick bulk region. Subtraction of the thickness of the bulk and two "surfaces" from the whole

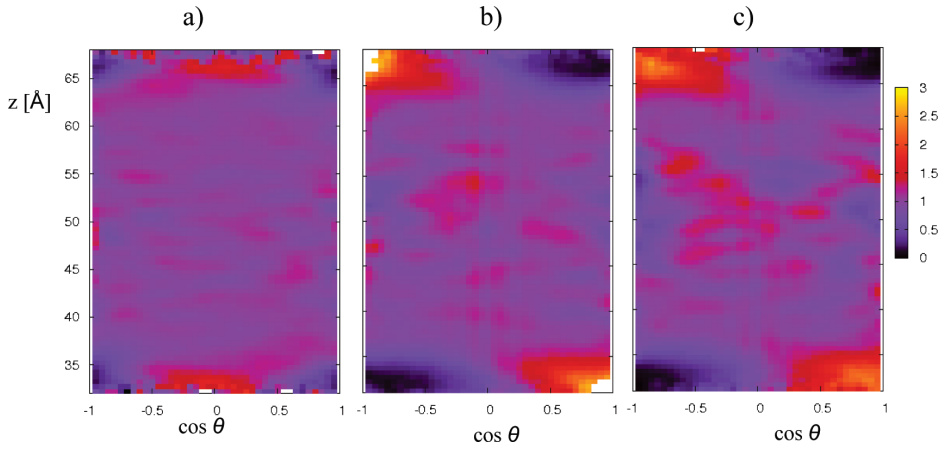

Figure 4. Orientation maps of dipoles of water molecules in supercooled liquid in neat water (a), water covered by pentanoic acid (b), and water covered by pentanol (c). Color coding corresponds to probability distribution as a function of z-coordinate (z-axis perpendicular to the interface) and cosine of the angle between the water dipole and z-axis. Brighter color means more probable orientation. Water molecules are oriented randomly in the bulk region. Surface water molecules have preferentially dipoles almost perpendicular to the z-axis in case of neat water (a). In polluted systems (b) and (c), water dipoles are mostly parallel to the z-axis with water molecules pointing with oxygen atoms toward the gas phase.

thickness, one obtains thickness of two "subsurfaces", 12−14 Å. Volumes of the bulk region and that of the two subsurface regions are roughly the same. It is worth mentioning that the terms "surface", "subsurface", and "bulk" not only have geometrical meaning but also correlate with properties of the hydrogen bond network.[47,48]

The next important observable is the mean time required for formation of either the subsurface or bulk nucleus. According to classical theories dealing with both volume or surface dependent nucleation,[4,55] we should obtain an exponential decrease from which we could extract the corresponding time constant. Characteristic nucleation times were obtained by least-squares fit of data (bulk and subsurface together) by $\exp(-t/\tau)$, where τ is characteristic nucleation time; this is a one-parameter fit. We also fitted data by $a[\exp(-t/\tau)]$ (two-parametr fit), but the difference between derived nucleation times was small. In all three systems, we also fitted bulk and subsurface data separately to see eventual difference, but they were negligible which means that the time required for formation of a subsurface nucleus does not differ significantly from that needed for formation of a bulk nucleus. Nucleation times are about 220 ns for both neat water and water covered by pentanoic acid, compared to 330 ns for water covered by pentanol. Note that the decay in Figure 3 is not perfectly exponential. Nevertheless, it can clearly be seen that nucleation in water covered by pentanol is slower than that in the other two cases.

After the nucleation event, ice starts to grow. The freezing rate, which is defined as the thickness of ice formed per time unit, is for neat water approximately 1 Å/ns, which is somewhat faster than typical experimental values. This is because in macroscopic experiments freezing is slowed down by the release of latent heat, which in a MD simulation of a small system is efficiently removed by the thermostat. The simulated freezing rate is practically unaffected by adding pentanoic acid, while it is slightly slowed down close to the water/pentanol interface.

Note that homogeneous ice nucleation observed in MD simulations possessing both bulk and surface regions is not just a special feature of the NE6 model. Already in our previous work,[35] we produced a successful nucleation trajectory employing the TIP5P model[36] at 240 K, which lies 35 K below its melting point. Most recently, we have obtained the first nucleation trajectory employing the TIP4P/2005[56] water model at 210 K, which is about 40 K below its melting point.

Discussion

We now discuss the different effects of pentanoic acid and pentanol on homogeneous ice nucleation. We start with the following question: How can we explain the negligible influence of pentanoic acid on the freezing process? First, note that pentanoic acid is a weak one; therefore, neglecting dissociation in the simulation does not cause a large error. Carboxylic acids form stable dimers with two strong hydrogen bonds, as well as reasonably stable (but weaker) heterodimers with water, as depicted in Figure 1a, b. In the heterodimer, pentanoic acid acts as a hydrogen bond donor. The pentanol dimer, in contrast to the acid one, contains only one hydrogen bond, being additionally stabilized by van der Waals interactions of alkyl chains (Figure 1c). Stabilization of this dimer is not as high as that of the pentanoic acid dimer. Pentanol and water form two heterodimers. The first one (Figure 1d) with water acting as a hydrogen bond donor is slightly more stable than the second one where pentanol is the hydrogen bond donor (Figure 1e). Summarizing these findings, it might be expected that the water surface is less affected by carboxylic acid, since the acid interacts more likely with other carboxylic acid molecules than with water molecules. We checked this hypothesis by hydrogen bond analysis, but, as a matter of fact, there is little difference between alcohol and acid in this respect. On average, one pentanoic acid molecule forms 2.3 hydrogen bonds with water (acting as hydrogen donor or hydrogen acceptor) and 0.2 hydrogen bonds with another acid, while pentanol forms 2.3 hydrogen bonds with water and 0.15 hydrogen bonds with another alcohol. Based on hydrogen bond analysis, we, therefore, cannot explain the different influence of alcohol versus acid on ice nucleation and, thus, have to look for other explanations.

Figure 4 depicts orientation maps of water dipoles with respect to the z-axis (i.e., the axis perpendicular to the interface). Orientation maps show "intensity" (number of molecules) as a function of z (axis perpendicular to the interface) and $\cos\theta$, where θ is an angle between the water dipole (pointing from oxygen to hydrogens) and z-direction. Prior to nucleation in bulk

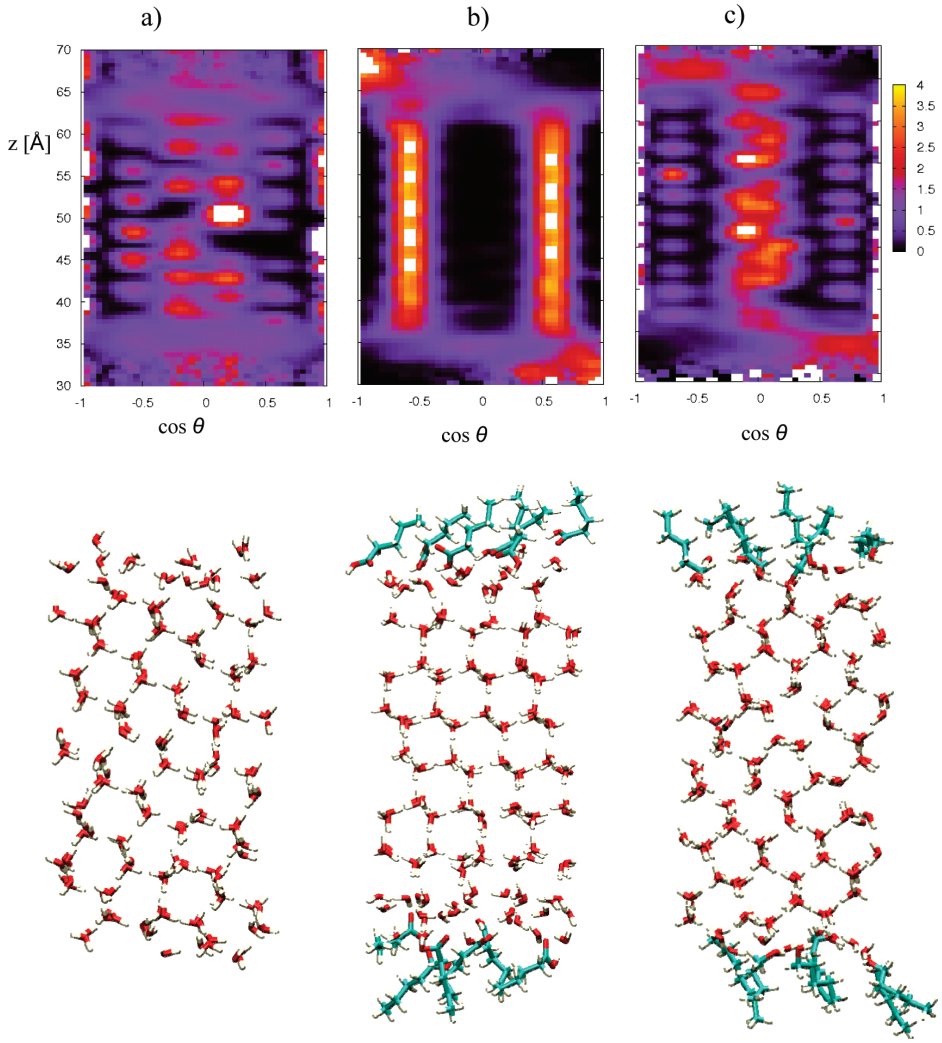

Figure 5. Orientation maps of dipoles of water molecules in frozen systems with corresponding snapshots: neat water (a), water covered with pentanoic acid (b), and water covered with pentanol (c). Color coding corresponds to probability distribution as a function of the z-coordinate (perpendicular to the interface) and the cosine of the angle between the water dipole and z-axis. Preferential orientation of interfacial water molecules does not change upon freezing (compare to Figure 4). Orientation of water molecules in ice is no more random as in the supercooled liquid, but it is determined by orientation of the basal plane with respect to the interface. Certain combinations of orientation and vertical position are more probable (brighter areas) and others less probable (dark areas) than those in bulk liquid.

water, all orientations of water molecules have the same probability, and therefore, the color of the corresponding area is uniform, but certain orientations are preferred at the interface. For example, water molecules expose oxygen to the adsorbate−water interface (Figure 4b, c); therefore, the probability of cos θ having a positive value (close to 1) is enhanced at the lower interface and the probability of cos θ having a negative value (close to −1) is enhanced at the upper interface. In the case of neat water, hydrogens are predominantly pointing toward the gas phase.

Orientation of molecules at the interface does not change after freezing, as can be seen from the upper part of Figure 5. This is because water molecules in the top layer remain unfrozen, forming a quasi-liquid layer. Orientation of water dipoles of surface molecules is thus similar for the two polluted systems but differs from that for neat water. Note also that orientation of water molecules in ice is no more random as in the supercooled liquid, but it is determined by orientation of the basal plane with respect to the interface. Certain combinations of orientation and vertical position are more probable (brighter areas) and others less probable (dark areas) than those in bulk liquid.

In all three investigated systems, homogeneous nucleation typically leads to formation of a mixture of cubic and hexagonal ice, while only rarely pure cubic or pure hexagonal ice is formed. This is in agreement with conclusions of other investigators[33] who observed that, regardless of the substrate, a variable number of stacking faults appear during crystallization. Our three investigated systems do not differ in crystal structure, but rather in orientation of the basal plane with respect to the interface. This plane is on average (over simulated trajectories) mainly tilted in the case of neat water (Figure 5a), both tilted and

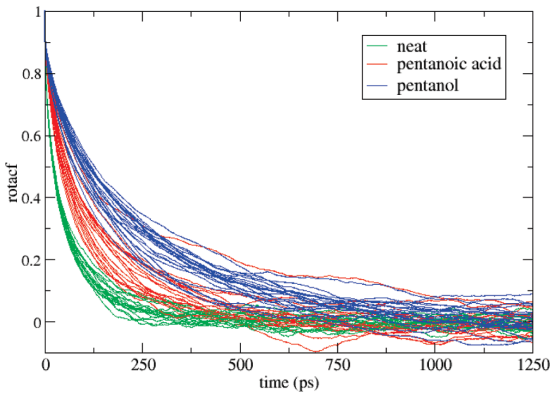

Figure 6. Average rotational autocorrelation function of eight most interfacial water molecules in neat water (green), water covered by pentanoic acid (red), and water covered by pentanol (blue). The correlation function was evaluated every 5 ns for the first 100 ns of the trajectory, that is why there are more lines for each system. No drift of correlation time with simulation time was observed.

coplanar in case of water covered by pentanol (Figure 5c), and mainly coplanar in case of water covered by pentanoic acid, which is illustrated in Figure 5b.

The increased rotational mobility of water molecules at the interface is important for homogeneous ice nucleation in the subsurface, since it represents a kinetic advantage (faster reorientation) for ice nucleation.[35] We have used the rotational autocorrelation function to represent mobility of interfacial water molecules, for which an almost exponential curve with fast decay was obtained for neat water, while for polluted systems rotation is more hindered. Figure 6 shows the average rotational autocorrelation function of eight most interfacial water molecules in all three investigated systems. In the case of neat water, correlation time is the shortest, with water molecules being more hindered for pentanol than pentanoic acid surface pollution.

While short-chain soluble alcohols act as antifreeze agents, it has been shown that ordered monolayers of long-chain aliphatic alcohols act as efficient ice nucleators,[13−20] which is rationalized in terms of a structural match between the monolayer and a layer of ice in the *ab* plane. The adsorbates investigated here lie in between these two limits. Pentanol molecules in our systems are strongly surface active but are not arranged in an ordered surface monolayer as in experiments with long-chain alcohols but rather form a disordered and incomplete layer, which then has a slowing rather than an enhancing effect on ice nucleation.

Conclusion

We have studied homogeneous ice nucleation in neat and surface contaminated water by means of extensive MD simulations. We did not want to draw conclusions from one or two trajectories, but aimed at bringing statistical averaging into this issue performing in total more then 60 simulations at the (sub)microsecond time scale. Nucleation preferentially starts in the subsurface in neat water and in water covered by pentanoic acid, with subsurface preference slightly decreased in the latter case. There is, however, virtually no preference for subsurface nucleation for water contaminated by pentanol. Nucleation times of neat water and water covered by pentanoic acid are practically the same (about 220 ns), while the presence of pentanol slows down nucleation by about 50%.

Based on our analysis of the MD trajectories, we come to the following conclusion. Neat water and water covered by pentanoic acid have similar kinetics of homogeneous ice nucleation but probably for different reasons. Adsorbates have an orientation effect, as demonstrated by orientation of water molecules at the interface and orientation of ice planes, which enhances ice nucleation. At the same time, adsorbates also hinder the motion of interfacial water molecules which slows down nucleation. These two effects practically compensate each other for water covered by pentanoic acid, while in the case of pentanol contamination hindering is stronger than the orientational effect, which is why the subsurface preference for nucleation is washed out and homogeneous ice nucleation is slower than that in neat water.

Acknowledgment. Support from the Czech Ministry of Education (Grants LC512) and from the US-NSF (Grant CHE0909227) is gratefully acknowledged. Access to the METACentrum supercomputing facilities provided under the research project MSM6383917201 is appreciated. E.P. acknowledges support from the International Max Planck Research School. L.V. acknowledges the receipt of the postdoctoral fellowship from the Alexander von Humboldt Foundation.

References and Notes

(1) Heymsfield, A. J.; Miloshevich, L. M. *J. Atmos. Sci.* **1993**, *50*, 2335.
(2) Rogers, D. C.; DeMott, P. J.; Kreidenweis, S.; Chen, Y. *Geophys. Res. Lett.* **1998**, *25*, 1383.
(3) Chang, H.-Y. A.; Koop, T.; Molina, L. T.; Molina, M. J. *J. Phys. Chem. A* **1999**, *103*, 2673.
(4) Pruppacher, H.; Klett, J. D. *Microphysics of Clouds and Precipitation*; Kluwer Academic Publishers: Dordrecht, 1998.
(5) Tabazadeh, A.; Djikaev, Y. S.; Reiss, H. *Proc. Natl. Acad. Sci. U.S.A.* **2002**, *99*, 15873.
(6) Duft, D.; Leisner, T. *Atmos. Chem. Phys.* **2004**, *4*, 1997.
(7) Koop, T. *Z. Phys. Chem.* **2004**, *218*, 1231.
(8) Lü, Y. J.; Xie, W. J.; Wei, B. *Appl. Phys. Lett.* **2005**, *87*, 184107.
(9) Kärcher, B.; Koop, T. *Atmos. Chem. Phys.* **2005**, *5*, 703.
(10) Prenni, A. J.; DeMott, P. J.; Kreidenweis, S. M.; Sherman, D. E.; Russell, L. M.; Ming, Y. *J. Phys. Chem. A* **2001**, *105*, 11240.
(11) Wise, M. E.; Garland, R. M.; Tolbert, M. A. *J. Geophys. Res.* **2004**, *109*, D19203.
(12) Szymer, W.; Zawadzki, I. *Bull. Am. Meteorol. Soc.* **1997**, *78*, 209.
(13) Gavish, M.; Popovitz-Biro, R.; Lahav, M.; Leiserowitz, L. *Science* **1990**, *250*, 973.
(14) Popovitz-Biro, R.; Wang, J. L.; Majewski, J.; Shavit, E.; Leiserowitz, L.; Lahav, M. *J. Am. Chem. Soc.* **1994**, *116*, 1179.
(15) Majewski, J.; Popovitz-Biro, R.; Kjaer, K.; Als-Nielsen, J.; Lahav, M.; Leiserowitz, L. *J. Phys. Chem.* **1994**, *98*, 4087.
(16) Majewski, J.; Popovitz-Biro, R.; Edgar, R.; Arbel-Haddad, M.; Kjaer, K; Bouwman, W.; Als-Nielsen, J.; Lahav, M.; Leiserowitz, L. *J. Phys. Chem. B* **1997**, *101*, 8874.
(17) Seeley, L. H.; Seidler, G. T. *J. Chem. Phys.* **2001**, *114*, 10464.
(18) Seeley, L. H.; Seidler, G. T. *Phys. Rev. Lett.* **2001**, *87*, 055702.
(19) Ochshorn, E.; Cantrell, W. *J. Chem. Phys.* **2006**, *124*, 054714.
(20) Zobrist, B.; Koop, T.; Luo, P. B.; Marcolli, C.; Peter, T. *J. Phys. Chem. C* **2007**, *111*, 2149.
(21) Dai, Y.; Evans, J. S. *J. Phys. Chem. B* **2001**, *105*, 10831.
(22) Nutt, D. R.; Stone, A. J. *J. Chem. Phys.* **2003**, *119*, 5670.
(23) Angell, C. A. Supercooled water. In *Water A Comprehensive Treatise*; Franks, F., Ed.; Plenum: New York, 1982.
(24) Krämer, B.; Hübner, O.; Vortisch, H.; Wöste, L.; Leisner, T.; Schwell, M.; Rühl, E.; Baumgärtel, H. *J. Chem. Phys.* **1999**, *111*, 6521.
(25) Wood, S. E.; Baker, M. B.; Swanson, B. D. *Rev. Sci. Instrum.* **2002**, *73*, 3988.
(26) Koop, T.; Bertram, A. K.; Molina, L. T.; Molina, M. J. *J. Phys. Chem. A* **1999**, *103*, 9042.
(27) Huang, J.; Bartell, L. S. *J. Phys. Chem.* **1995**, *99*, 3924.
(28) Bauerecker, S.; Ulbig, P.; Buch, V.; Vrbka, L.; Jungwirth, P. *J. Phys. Chem. C* **2008**, *112*, 7631.
(29) Jorgensen, W. L.; Chandrasekhar, J.; Madura, J. D.; Impey, R. W.; Klein, M. L. *J. Chem. Phys.* **1983**, *79*, 926.
(30) Matsumoto, M.; Saito, S.; Ohmine, I. *Nature* **2002**, *416*, 409.
(31) Nada, H.; van der Eerden, J. P. J. M. *J. Chem. Phys.* **2003**, *118*, 7401.

(32) Nada, H.; van der Eerden, J. P.; Furukawa, Y. *J. Cryst. Growth* **2004**, *266*, 297.
(33) Carignano, M. *J. Phys. Chem. C* **2007**, *111*, 501.
(34) Nada, H.; Furukawa, Y. *J. Phys. Chem. B* **2008**, *112*, 7111.
(35) Vrbka, L.; Jungwirth, P. *J. Phys. Chem. B* **2006**, *110*, 18126.
(36) Mahoney, M. W.; Jorgensen, W. L. *J. Chem. Phys.* **2000**, *112*, 8910.
(37) Li, Y.-C.; Yu, J. Z. *Environ. Sci. Technol.* **2005**, *39*, 7616.
(38) Vaida, V.; A. F. Tuck, A. F.; Ellison, G. B. *Phys. Chem. Earth, Part C* **2000**, *25*, 195.
(39) BinAbas, M. R.; Simoneit, B. R. T. *Atmos. Environ.* **1996**, *30*, 2779.
(40) Simoneit, B. R.T.; Mazurek, M. A. *Atmos. Environ.* **1982**, *16*, 2139.
(41) Romero, C. M.; Suárez, F. *J. Solution Chem.* **2009**, *38*, 315.
(42) Pai, Y.-H.; Chen, L.-J. *Fluid Phase Equilib.* **1999**, *155*, 95.
(43) Abascal, J. L. F.; Sanz, E.; Fernandez, R. G.; Vega, C. *J. Chem. Phys.* **2005**, *122*, 234511.
(44) Abascal, J. L. F.; Fernández, R. G.; Vega, C. J.; Carignano, M. A. *J. Chem. Phys.* **2006**, *125*, 166101.
(45) Nada, H.; Furukawa, F. *J. Cryst. Growth* **2005**, *283*, 242.
(46) Wang, J.; Cieplak, P.; Kollman, P. A. *J. Comput. Chem.* **2000**, *21*, 1049.
(47) Kuo, I. F.-W.; Mundy, J. C. *Science* **2004**, *303*, 658.
(48) Wilson, M. A.; Pohorille, A; Pratt, L. R. *J. Phys. Chem.* **1987**, *91*, 4873.
(49) Yeh, I.-C.; Berkowitz, M. L. *J. Chem. Phys.* **1999**, *111*, 3155.
(50) Hess, B.; Bekker, H.; Berendsen, H. J. C.; Fraaije, J. G. E. M. *J. Comput. Chem.* **1997**, *18*, 1463.
(51) Nose, S. *Mol. Phys.* **1984**, *52*, 255.
(52) Lindahl, E.; Hess, B.; van der Spoel, D. *J. Mol. Model.* **2001**, *7*, 306.
(53) Fernández, R. G.; Abascal, J. L. F.; Vega, C. *J. Chem. Phys.* **2006**, *124*, 144506.
(54) Vrbka, L.; Jungwirth, P. *J. Mol. Liq.* **2007**, *134*, 64.
(55) Volmer, M. *Kinetic der Phasenbildung*; Steinkopf: Leipzig, 1939.
(56) Abascal, J. L. F.; Vega, C. *J. Chem. Phys.* **2005**, *122*, 234505.

JP9090238

Bibliography

[1] Petrenko, V. F.; Whitworth, R. W. *Physics of Ice*, Oxford University Press, Inc., New York **1999**.

[2] Proceeding of the 18^{th} International Conference of Nucleation and Atmospheric Aerosols edited by Jiří Smolík and Colin O'Dowd **2009**, Prague.

[3] Heymsfield, A. J.; Miloshevich, L. M. *J. Atmos. Sci* **1993**, *50*, 2335.

[4] Chang, H.-Y. A.; Koop, T.; Molina, L. T.; Molina, M. J. *J. Phys. Chem. A* **1999**, *103*, 2673.

[5] Rogers, D. C.; DeMott, P. J.; Kreidenweis, S.; Chen, Y. *Geophys. Res. Lett* **1998**, *25*, 1383.

[6] Pruppacher, H. D.; Klett, J. D. *Microphysics of Clouds and Precipitation* **1997**, Kluwer Academic Publishers, Dordrecht.

[7] Koop, T. *Z. Phys. Chem* **2004**, *218*, 1231.

[8] Tabazadeh, A.; Djikaev, Y. S.; Reiss, H. *Proc. Nat. Acad. Sci. USA* **2002**, *99*, 15873.

[9] Matsumoto, M.; Saito, S.; Ohmine, I. *Nature* **2002**, *416*, 409.

[10] Vrbka, L.; Jungwirth, P. *J. Phys. Chem. B* **2006**, *110*, 18126.

[11] Volmer, M. *Kinetik der Phasenbildung*, Steinkoff, Leipzig **1939**.

[12] Djikaev, Y. S.; Tabazadeh, A.; Hamill, P.; Reiss, H. *J. Phys. Chem. A* **2002**, *106*, 10247.

[13] Tabazadeh, A.; Djikaev, Y. S.; Hamill, P.; Reiss, H. *J. Phys. Chem. A* **2002**, *106*, 10238.

[14] Rasmussen, D. H. *J. Cryst. Crowth* **1982**, *56*, 56.

[15] Murray, B. J.; Knopf, D. A.; Bertram, A. K. *Nature* **2005**, *434*, 202.

[16] Szyrmer, W.; Zawadzki, I. *Bull. Amer. Meteor. Soc.* **1997**, *78*, 209. and references there in.

[17] Vaida, V.; Tuck, A. F.; Ellison, G. B. *Phys. Chem. Earth Part C* **2000**, *25*, 195.

[18] Angell, C. A. *Supercooled water* in *Water a comprehensive treatise* F. Franks (Ed.) **1982**, *86*, 982.

[19] Wood, S. E.; Baker, M. B.; Swanson, B. D. *Rev. Sci. Instrum.* **2002**, *73*, 3988.

[20] Krämer, B.; Hübner, O.; Vortisch, H.; Wöste, L.; Leisner, T.; Schwell, M.; Rühl, E.; Baumgärtel, H. *J. Chem. Phys.* **1999**, *111*, 6521.

[21] Stöckel, P.; Weidinger, I. M.; Baumgärtel, H.; Leisner, T. *J. Phys. Chem. A* **2005**, *109*, 2540.

[22] Huang, J.; Bartell, L. S. *J. Phys. Chem.* **1995**, *99*, 3924.

[23] Bauerecker, S.; Ulbig, P.; Buch V.; Vrbka, L.; Jungwirth, P. *J. Phys. Chem. C* **2008**, *112*, 7631.

[24] Duft, D.; Leisner, T. *Atmos. Chem. Phys.* **2004**, *4*, 1997.

[25] Popovitz-Biro, R.; Wang, J. L.; Majewski, J.; Shavit, E.; Leiserowitz, L.; Lahav, M. *J. Am. Chem. Soc.* **1994**, *116*, 1179.

[26] Zobrist, B.; Koop, T.; Luo, P. B.; Marcolli, C.; Peter, T. *J. Phys. Chem. C* **2007**, *111*, 2149.

[27] Gavish, M.; Popovitz-Biro, R.; Lahav, M.; Leiserowitz, L. *Science* **1990**, *250*, 973.

[28] Majewski, J.; Popovitz-Biro, R.; Kjaer, K.; Als-Nielsen, J.; Lahav, M.; Leiserowitz, L. *J. Phys. Chem.* **1994**, *98*, 4087.

[29] Majewski, J.; Popovitz-Biro, R.; Edgar, R.; Arbel-Haddad, M.; Kjaer, K; Bouwman, W.; Als-Nielsen, J.; Lahav, M.; Leiserowitz, L. *J. Phys. Chem. B* **1997**, *101*, 8874.

[30] Seeley, L. H.; Seidler, G. T. *J. Chem. Phys.* **2001**, *114*, 10464.

[31] Seeley, L. H.; Seidler, G. T. *Phys. Rev. Lett.* **2001**, *87*, 055702.

[32] Ochshorn, E.; Cantrell, W. *J. Chem. Phys* **2006**, *124*, 054714.

[33] Jorgensen, W. L.; Chandrasekhar, J.; Madur J. D.; Impey, R. W.; Klein, M. L. *J. Chem. Phys.* **1983**, *79*, 926.

[34] Nada, H.; van der Eerden, J. P. J. M. *J. Chem. Phys.* **2003**, *118*, 7401.

[35] Nada, H.; van der Eerden J. P.; Furukawa, Y. *J. Crystal Growth* **2004**, *266*, 297.

[36] Carignano, M. *J. Phys. Chem. C* **2007**, *111*, 501.

[37] Nada, H., Furukawa, Y. *J. Phys. Chem. B* **2008**, *112*, 7111.

[38] Dai, Y.; Evans, J. S. *J. Phys. Chem. B.* **2001**, *105*, 10831.

[39] Nutt, D. R.; Stone, A. J. *J. Chem. Phys.* **2003**, *119*, 5670 .

[40] Malijevský, A. *Lekce ze statistické termodynamiky*, 3rd edition, VŠCHT Praha **2009**.

[41] Cramer, C. J. *Essentials of Computational Chemistry*, Willey Sons, **2004**.

[42] Nezbeda, I.; Kolafa, J.; Kotrla, M. *Úvod do počítačových simulací, Metody Monte Carlo a molekulární dynamiky*, Karolinum, UK v Praze **2003**.

[43] Jungwirth, P., *Klasická a kvantová molekulová dynamika*, www.molecular.cz/∼jungwirt.

[44] McQuarrie, D. A. *Statistical mechanics*, University Science Books, Sausalito, California **2000**.

[45] Ryckaert, J. P; Ciccotti, G.; Berendsen, J. H. C. *J. Comp. Phys.* **1997**, *23*, 327.

[46] Hess, B.; Bekker, H.; Berendsen, H. J. C.; Fraaije, J. G. E. M. *J. Comp. Chem.* **1997**, *18*, 1463.

[47] Lindahl, E.; Hess, B.; van der Spoel, D. *J. Mol. Mod.* **2001**, *7*, 306.

[48] Hess, R.; Kutzner, C.; van der Spoel, D.; Lindahl, E. . *J. Chem. Theory Comput.* **2008**, *4*, 435.

[49] Frisch, M. J.; Trucks, G. W.; Schlegel, H. B.; Scuseria, G. E.; Robb, M. A.; Cheese-man, J. R.; Montgomery, J. A., Jr.; Vreven; T., Kudin; K. N., Burant, J. C.; Millam, J. M.; Iyengar, S. S.; Tomasi, J.; Barone, V.; Mennucci, B.; Cossi, M.; Scalmani, G.; Rega, N.; Petersson, G. A.; Nakatsuji, H.; Hada, M.; Ehara, M.; Toyota, K.; Fukuda, R.; Hasegawa, J.; Ishida, M.; Nakajima, T.; Honda, Y.; Kitao, O.; Nakai, H.; Klene, M.; Li, X.; Knox, J. E.; Hratchian, H. P.; Cross, J. B.; Bakken, V.; Adamo, C.; Jaramil-lo, J.; Gomperts, R.; Stratmann, R. E.; Yazyev, O.; Austin, A. J.;Cammi, R.; Pomelli, C.; Ochterski, J. W.; Ayala, P. Y.; Morokuma, K.; Voth, G. A.; Salvador, P.; Dannen-berg, J. J.; Zakrzewski, V. G.; Dapprich, S.; Daniels, A. D.; Strain, M. C.; Farkas, O.; Malick, D. K.; Rabuck, A. D.; Raghavachari, K.; Foresman, J. B.; Ortiz, J. V.; Cui, Q.; Baboul, A. G.; Clifford, S.; Cioslowski, J.; Stefanov, B. B.; Liu, G.; Liashenko, A.; Piskorz, P.; Komaromi, I.; Martin, R. L.; Fox, D. J.; Keith, T.; Al-Laham, M. A.; Peng, C. Y.; Nanayakkara, A.; Challacombe, M.; Gill, P. M. W.; Johnson, B.; Chen, W.; Wong, M. W.; Gonzalez, C.; Pople; J. A., *Gaussian 03, Revision E.01, Gaussian*, Inc., Wallingford CT,**2004**.

[50] Berendsen, H. J. C.; Postma, J. P. M.; van Gunsteren, W. F.; Hermans, J. in *Intermolecular Forces* edited by Pullman, B., Reidel, Dortrecht **1982**, pp. 331 .

[51] Berendsen, H. J. C.; Grigera, J. R.; Straatsma, T. P. *J. Phys. Chem.* **1987**, *91*, 6269.

[52] Jorgensen, W. L.; Chandrasekhar, J. D.; Madura, J. D.; Impey, R. W.; Klein, M. L. *J.Chem. Phys.* **1983**, *79*, 926.

[53] Abascal, J. L. F.; Sanz, E.; Fernández, R. G.; Vega, C. *J. Chem. Phys* **2005**, *122*, 234511.

[54] Abascal, J. L. F.; Vega, C.*J. Chem. Phys.* **2005**, *123*, 234505.

[55] Horn, H. W.; Swope, W. C; Pitera, J. W.; Madura, J. D.; Dick,T. J.; Hura, G. L.; Head-Gordon, T. *J. Chem. Phys.* **2002**, *258*, 121.

[56] Mahoney, M. W.; Jorgensen, W. L. *J. Chem. Phys.* **2000**, *112*, 8910.

[57] Nada, H.; Furukawa, Y. *J. Cryst. Growth* **2005**, *283*, 242.

[58] Abascal, J. L. F.; Fernández, R. G.; Vega, C. J.; Carignano, M. A. *J. Chem. Phys* **2006**, *125*, 166101.

[59] Wang, J.; Cieplak, P.; Kollmann, P. A. *J. Comp. Chem.* **2000**, *21*, 1049.

[60] Singh, U. C.; Kollmann, P. A. *J. Comp. Chem.* **1984**, *5*, 129.

[61] Xanteas, S. S.; Burnham, C. J.; Harrison, R. J. *J. Phys. Chem.* **2002**, *16*, 1493.

[62] Kuo, I. F.– .W.; Mundy, J. C. *Science* **2004**, *303*, 658.

[63] Wilson, M. A.; Pohorille, A.; Pratt, L. R. *J. Phys. Chem.* **1987**, *91*, 4873.

[64] Berendsen, H. J. C.; Postma, J. P. M.; van Gunsteren, W. F.; Dinola, A.; Haak, J. R. *J. Chem. Phys.* **81** (1984) 3684.

[65] Nose, S. *Mol. Phys.* **1984**, *52*, 255 and Hoover, G., W. *Phys. Rew.* **1985**, *31*, 1695.

[66] Yeh, I.-C.; Berkowitz, M. L. *J. Chem. Phys.* **1999**, *111*, 3155.

[67] Vrbka, L.; Jungwirth, P. *J. Mol. Liq.* **2007**, *134*, 64.

[68] Fernández, R. G.; Abascal, J. L. F.; Vega, C. *J. Chem. Phys.* **2006**, *124*, 144506.